bioRxiv preprint doi: https://doi.org/10.1101/2020.11.24.395954; this version posted November 24, 2020. The copyright holder for this preprint (which was not certified by peer review) is the author/funder. All rights reserved. No reuse allowed without permission.

The *Physcomitrium (Physcomitrella) patens* PpKAI2L receptors for strigolactones and related compounds highlight MAX2 dependent and independent pathways

Mauricio Lopez-Obando[1,2,3,7], Ambre Guillory[1,7], François-Didier Boyer[4], David Cornu[5], Beate Hoffmann[1], Philippe Le Bris[1], Jean-Bernard Pouvreau[6], Philippe Delavault[6], Catherine Rameau[1], Alexandre de Saint Germain[1]*, Sandrine Bonhomme[1]*

[1] Institut Jean-Pierre Bourgin, INRAE, AgroParisTech, Université Paris-Saclay, 78000 Versailles, France

[2] Department of Plant Biology, Swedish University of Agricultural Sciences, The Linnean Centre for Plant Biology in Uppsala, SE-750 07, Uppsala, Sweden

[3] VEDAS Corporación de Investigación e Innovación (VEDASCII), Cl 8 B 65-261 050024, Medellín, Colombia

[4] Université Paris-Saclay, CNRS, Institut de Chimie des Substances Naturelles, UPR 2301, 91198, Gif-sur-Yvette, France

[5] Université Paris-Saclay, CEA, CNRS, Institute for Integrative Biology of the Cell (I2BC), 91198, Gif-sur-Yvette, France

[6] Université de Nantes, Laboratoire de Biologie et Pathologie Végétales, LBPV, EA1157, 44000, Nantes, France

[7] These authors equally contributed to this work

*Corresponding authors

Short title: Defining receptors to strigolactones in *P. patens*

bioRxiv preprint doi: https://doi.org/10.1101/2020.11.24.395954; this version posted November 24, 2020. The copyright holder for this preprint (which was not certified by peer review) is the author/funder. All rights reserved. No reuse allowed without permission.

ABSTRACT

In flowering plants, the α/β hydrolase DWARF14 (D14) perceives strigolactone (SL) hormones and interacts with the F-box protein MORE AXILLARY GROWTH2 (MAX2) to regulate developmental processes. The key SL biosynthetic enzyme, CAROTENOID CLEAVAGE DEOXYGENASE8 (CCD8), is present in the moss *Physcomitrium (Physcomitrella) patens*, and PpCCD8-derived compounds regulate plant extension. However, perception of these still unknown compounds does not require the PpMAX2 homolog. Putative candidate receptors are among the 13 *PpKAI2LIKE-A to -L* genes, homologous to the ancestral *D14* paralog *KARRIKIN INSENSITIVE2* (*KAI2*). In Arabidopsis, AtKAI2 is the receptor for karrikins and a still elusive endogenous KAI2-Ligand (KL). Based on germination assays using seeds of the parasitic plant *Phelipanche ramosa*, we propose that PpCCD8-derived compounds are non-canonical SLs. We show that all tested PpKAI2L proteins can bind and cleave SL analogs, some with similar affinities to AtKAI2. The PpKAI2L-H protein shows a strong hydrolytic activity not found for other PpKAI2L. Moss mutants for all *PpKAI2L* gene subclades were obtained and tested for their response to SL analogs. We show that *PpKAI2L-A to -E* genes encode redundant proteins that are not involved in PpCCD8-derived compound perception, but rather act in a PpMAX2-dependant pathway. In contrast, mutations in *PpKAI2L-G*, and *-J* genes abolish the response to the SL analog (+)-GR24, suggesting that both these encoded proteins are receptors for PpCCD8-derived molecules.

INTRODUCTION

Strigolactones (SLs) are butenolide compounds with dual roles in plants: exuded in soil, SLs signal the presence of a host to Arbuscular Mycorrhizal (AM) fungi (Akiyama et al. 2005; Besserer et al. 2006), and thus favor the establishment of symbiosis; as endogenous compouds, they (or derived compounds) play a hormonal role in developmental programs (Gomez-Roldan et al. 2008; Umehara et al. 2008) for reviews: (Lopez-Obando et al. 2015; Waters et al. 2017). SLs exuded from plant roots also act as signalling molecules in the rhizosphere inducing parasitic plant seed germination (Cook et al. 1966) for review: (Delavault 2017). SLs have been found in most land plants, including bryophytes, lycophytes, gymnosperms, and angiosperms (Yoneyama et al. 2018a). However, their synthesis and signaling pathways are mainly described in angiosperms where core enzyme pathways have

bioRxiv preprint doi: https://doi.org/10.1101/2020.11.24.395954; this version posted November 24, 2020. The copyright holder for this preprint (which was not certified by peer review) is the author/funder. All rights reserved. No reuse allowed without permission.

been identified, among which two CAROTENOID CLEAVAGE DEOXYGENASEs (CCD7 and CCD8) convert carotenoids into carlactone (CL). CL is the reported precursor of all known SLs, and the substrate for further enzymes such as the CYTOCHROME-P450 MORE AXILLARY GROWTH1 (MAX1) (for review: (Alder et al. 2012; Al-Babili and Bouwmeester 2015). Depending on the plant species, CL is converted into canonical or non-canonical SLs. These differ in the structure attached to the conserved enol ether-D ring moiety, shared by all SLs, and essential for biological activity (Yoneyama et al. 2018a; Yoneyama 2020). In angiosperms, SLs are perceived by an α/β hydrolase DWARF14 (D14)/DECREASED APICAL DOMINANCE2 (DAD2) that interacts with an F-box protein MORE AXILLARY GROWTH2 (MAX2) to target repressor proteins for proteasome degradation (Soundappan et al. 2015; Waters et al. 2015a). The originality of SL perception is that the D14 protein is both a receptor and an enzyme that cleaves its substrate (and covalently binds part of the SL), in a mechanism that is still under debate (Yao et al. 2016; de Saint Germain et al. 2016; Shabek et al. 2018; Seto et al. 2019) and for review:(Bürger and Chory 2020).

The evolutionary origins of SLs, and in particular whether their primary role is as a hormone or rhizospheric signal are still unclear. SL identification and quantification is a challenge in many species, due to the very low amounts of the molecules present in plant tissues or exudates, and their high structural diversification (Xie 2016; Yoneyama et al. 2018b). Therefore, the occurrence of SLs in a species was often inferred from the presence of the core biosynthesis enzymes in its genome (Delaux et al. 2012; Walker et al. 2019). Recently SLs were proposed to only be produced in land plants (Walker et al. 2019). Evidence of an ancestral pathway to SL pathway came from the identification of an ancient D14 paralog named KARRIKIN INSENSITIVE2/HYPOSENSITIVE TO LIGHT (KAI2/HTL) (Nelson et al. 2011; Waters et al. 2012) during screening of Arabidopsis mutants. KAI2 is also an α/β hydrolase like D14, that also interacts with the MAX2 F-box protein, in a pathway regulating Arabidopsis seed germination and seedling development. However, the endogenous signal perceived through this pathway remains unknown and is reported thus far as the KAI2-Ligand (KL) (Conn and Nelson 2015). KAI2 is also involved in stress tolerance, drought tolerance and AM symbiosis (Gutjahr et al. 2015; Wang et al. 2018; Villaecija-Aguilar et al. 2019; Li et al. 2020).

To gain insight into SL signaling evolution, we focused our studies on a model for the earliest land plants, namely *Physcomitrium (Physcomitrella) patens* (*P. patens*). As a moss, *P. patens*

bioRxiv preprint doi: https://doi.org/10.1101/2020.11.24.395954; this version posted November 24, 2020. The copyright holder for this preprint (which was not certified by peer review) is the author/funder. All rights reserved. No reuse allowed without permission.

belongs to the bryophytes, which also includes two other clades, hornworts and liverworts (Bowman et al. 2019). Bryophytes are currently described as a monophyletic group of embryophytes sharing an ancestor with vascular plants (Puttick et al. 2018; Harris et al. 2020). Extant bryophytes are therefore considered the descendants of the first plants able to survive out of water, and conquer land, 450 million years ago (Bowman et al. 2019; Blázquez et al. 2020; Harris et al. 2020). In *P. patens*, both the PpCCD7 and PpCCD8 enzymes required for SL synthesis are found (Proust et al. 2011), and carlactone has been detected as the product of PpCCD8 (Decker et al. 2017). The extended phenotype of *Ppccd8* mutant plants indicates that PpCCD8-derived molecules are required for moss filament growth regulation, and more broadly for interaction with neighboring plants (Proust et al. 2011). Application of the artificial SL, (±)-GR24, complements the *Ppccd8* mutant phenotype (Proust et al. 2011). PpCCD8-derived molecules also appear to play a role in rhizoid elongation and gametophore shoot branching (Delaux et al. 2012; Coudert et al. 2015). However, the exact nature of PpCCD8-derived molecules is still elusive (Yoneyama et al. 2018b) and the absence of *MAX1* homologs in *P. patens* suggests that the synthesis pathway in moss may differ from that of vascular plants. Nevertheless, phylogenetic analysis of *MAX1* homologs highlights the presence of this gene in other mosses and suggests that the biosynthesis pathway is conserved in land plants (Walker et al. 2019). Contrary to its flowering plant homolog, PpMAX2 is not involved in the perception of PpCCD8-derived molecules, as the corresponding mutant does respond to (±)-GR24 (Lopez-Obando et al. 2018). The PpMAX2 F-box protein appears to be involved in a light dependent pathway required for moss early development and gametophore development regulation (number and size) (Lopez-Obando et al. 2018). In initial studies no true homolog for the D14 SL receptor was found in the *P. patens* genome, whereas 11-13 *PpKAI2-LIKE* (*PpKAI2L*) candidate genes, named *PpKAI2L-A* to *PpKAI2L-M*, were described (Lopez-Obando et al. 2016a). These genes are grouped into four subclades (i), (i.i-i.ii), (ii) and (iii), hereafter renamed as PpKAI2L-(A-E), (FK), (HIL), and (JGM), respectively. A comprehensive phylogenetic assessment placed the *P. patens* clades (FK), (HIL), and (JGM) into a super clade called DDK (D14/DLK2/KAI2) containing spermatophyte (angiosperm and gymnosperm) D14 clades, while clade (A-E) belongs to the EuKAI2 clade, common to all land plants (Bythell-Douglas et al. 2017). Nevertheless, moss proteins from the DDK clade were found to be as different from D14 as from KAI2 (Bythell-Douglas et al. 2017). Prediction of PpKAI2L protein structures found various pocket sizes, as observed for D14 and KAI2 from vascular plants (Lopez-Obando et al. 2016a). Consequently, those (or some of those) genes could encode

bioRxiv preprint doi: https://doi.org/10.1101/2020.11.24.395954; this version posted November 24, 2020. The copyright holder for this preprint (which was not certified by peer review) is the author/funder. All rights reserved. No reuse allowed without permission.

receptors for various molecules, including the PpCCD8-derived compounds, or the elusive KL (Conn and Nelson 2015). Accordingly, in our study of PpMAX2 we hypothesized that this F-box protein might be involved in a moss KL pathway (Lopez-Obando et al. 2018). But the question as to the involvement of PpKAI2L proteins in the PpMAX2 pathway remains open. Last year, the crystal structures of PpKAI2L-C, -E and -H were published (Bürger et al. 2019). In addition, it was shown that *in vitro* purified PpKAI2L proteins -C, -D and -E bind (–)-5-deoxystrigol, a canonical SL with non-natural stereochemistry. In contrast, PpKAI2L proteins -H, -K and -L could adapt the karrikin KAR_1 (Bürger et al. 2019). However, proteins from the (JGM) clade were not studied, and no evidence for a role of one (or several) PpKAI2L as receptors for CCD8-derived molecules was provided, nor were *in vivo* (in moss) experiments carried out to validate the results.

There are thus several unresolved questions remaining to understand the evolution of the SL signaling pathway. The aim of the present study was to investigate the nature of the PpCCD8-derived molecules in moss and identify the receptors for these compounds. These goals would be facilitated by using a mimic of these molecules in assays. So far, the racemic (±)-GR24 has been used as an analog to SLs, but recent reports found that the different enantiomers present in this synthetic mixture do not have the same effect (Scaffidi et al. 2014). Indeed, (+)-GR24, (also called $GR24^{5DS}$) with a configuration close to the natural strigol is mostly perceived by D14 and mimics CCD8-derived SLs (e.g. carlactone). On the other hand, the configuration of (–)-GR24 (also called $GR24^{ent\text{-}5DS}$) has so far not been found in natural SLs. However, KAI2 perceives the (–)-GR24 analog better than D14 proteins and has been described as a KL mimic (Scaffidi et al. 2014; Zheng et al. 2020).

Here we tested the activity of *P. patens* as a stimulant for *P. ramosa* germination, in an attempt to shed light on the chemical nature of PpCCD8-derived compounds. We also characterized the expression patterns of all 13 *PpKAI2L* genes in moss, at various developmental stages. Refining the findings of (Bürger et al. 2019), we assessed the biochemical activity of PpKAI2L proteins *in vitro* by testing their cleavage activity and binding to both GR24 enantiomers. We expressed some of these proteins in the Arabidopsis *d14-1 kai2-2* double mutant to examine conservation of the SL and/or KL perception function. Finally, we used CRISPR-Cas9 technology to isolate *P. patens* mutants amongst the four clades of *PpKAI2L* genes, and analyzed their phenotype and their response to both GR24 enantiomers. We propose that clade (A-E) PpKAI2L proteins could be moss KL receptors, while clade (JGM) PpKAI2L would function as PpCCD8-derived compound receptors.

bioRxiv preprint doi: https://doi.org/10.1101/2020.11.24.395954; this version posted November 24, 2020. The copyright holder for this preprint (which was not certified by peer review) is the author/funder. All rights reserved. No reuse allowed without permission.

RESULTS

PpCCD8-derived compounds induce the germination of a hemp-specific population of *Phelipanche ramosa*

Yoneyama et al (Yoneyama et al. 2018b) indicated that the canonical SLs previously reported in moss tissues (Proust et al. 2011) could be contaminants. However other evidence suggests that *P. patens* does synthesize SL-like products. Indeed, PpCCD8 shows carlactone synthase activity (Decker et al. 2017), and both the synthetic SL analog (±)-GR24 and carlactone do complement the *Ppccd8* phenotype (Proust et al. 2011; Decker et al. 2017). Still, quantification of SL and related compounds is a challenge in many species (Boutet-Mercey et al. 2018; Yoneyama et al. 2018b; Floková et al. 2020; Rial et al. 2019), and despite many attempts with recent technologies and standards, so far no known SL has been identified from *P. patens* (Yoneyama et al. 2018b). An alternative to evaluate the SL-like activity of PpCCD8-derived molecules is to test the ability of *P. patens* exudates to induce the germination of parasitic seeds. Parasitic plants such as *Phelipanche ramosa* can parasitize various host plants, in response to specific exuded germination stimulants (GS). Different genetic groups of *P. ramosa* seeds have been identified, depending on the crop grown in the field where the seeds were collected (Huet et al. 2020). Seeds from two populations of *P. ramosa* harvested in hemp (*P. ramosa* group 2a) and oilseed rape (*P. ramosa* group 1) fields (Stojanova et al. 2019; Huet et al. 2020) were assayed with WT moss exudates. As a control, both groups of seeds were germinated in the presence of (±)-GR24 (Figure 1A). WT moss exudates induced germination of *P. ramosa* group 2a seeds but not *P. ramosa* group 1 seeds (Figure 1A). In another assay, *P. ramosa* seeds were added to culture plates close to WT or *Ppccd8* plants, with and without (±)-GR24 (Figure 1B-C). *P. ramosa* group 2a but not group1 seeds germinated on WT moss plates, while no germination was observed in the vicinity of *Ppccd8* plants. In all cases (WT and *Ppccd8*), the addition of (±)-GR24 to the medium restored seed germination. Thus, PpCCD8-derived compounds induce the germination of a specific population of *P. ramosa* seeds, responding to GS exuded by hemp.

P. patens responds strongly to (+)-GR24 and carlactone application, but poorly to (–)-GR24 and KAR_2 in the dark

bioRxiv preprint doi: https://doi.org/10.1101/2020.11.24.395954; this version posted November 24, 2020. The copyright holder for this preprint (which was not certified by peer review) is the author/funder. All rights reserved. No reuse allowed without permission.

The length of *caulonema* filaments grown in the dark has been used as a proxy for quantifying the *P. patens* phenotypic response to SL using (±)-GR24 in Petri dish assays (Hoffmann et al. 2014; Lopez-Obando et al. 2018). Here we used 24-well tissues culture plates, which reduced the amount of compound required for phenotypic assays (Guillory and Bonhomme 2021), and the number of caulonemal filaments per plant ended up a more robust proxy of the response to compounds than *caulonema* length (Figure 2 and Supplemental Figure 1). Since it is now well established that (±)-GR24 can activate non-specific responses (Scaffidi et al. 2014), we tested the (+) and (–)-GR24 enantiomers separately on both WT and the *Ppccd8* mutant. As in previous studies (Hoffmann et al. 2014; Lopez-Obando et al. 2018), we predicted a clearer response in the synthesis mutant than in the WT, due to the absence of endogenous PpCCD8-derived compounds potentially mimicked by (+)-GR24. Both the number and the length of *caulonema* filaments significantly decreased following application of (+)-GR24 in WT and the *Ppccd8* mutant, in a dose-response manner (Figure 2 and Supplemental Figure 1). A dose of 0.1 µM was sufficient to see a clear and significant response in terms of number in both genotypes (Figure 2). Application of (–)-GR24 led to a significant decrease in *Ppccd8* filament length, as did (+)-GR24, but there was no effect on WT filament length (Supplemental Figure 1). Strikingly, no significant changes in *caulonema* filament number were observed with (–)-GR24, except in WT for which the 0.1 µM and 10 µM doses led to a significant increase (more pronounced at 0.1 µM, Figure 2A). However, in further assays (see below, Figure 11), a slight but significant decrease of *Ppccd8 caulonema* filament number was observed following (–)-GR24 application. In summary, the phenotypic response of *P. patens* to (+)-GR24 was pronounced and significant with a decrease in both filament number and length in WT and *Ppccd8*. The response to (–)-GR24 was less clear for both genotypes, with sometimes contradictory effects (increase of number in WT, see above).

A previous study concluded that there was no KAR_1 response in either WT or the *Ppccd8* mutant, when *caulonema* length was observed in the dark or a transcriptional marker was used (Hoffmann et al. 2014). In the present work, we tested the KAR_2 molecule because it was described as being more active than KAR_1 in Arabidopsis (Sun et al. 2020) (Figure 2A-B). KAR_2 has an unmethylated butenolide group, unlike KAR_1. In WT, no significant effect on *caulonema* number was observed following application of increasing doses of KAR_2 (Figure 2A). In *Ppccd8*, we observed an increase in filament number, as with (–)-GR24 in WT, and this increase was significant at 10 µM (Figure 2B). Surprisingly, the length of WT filaments decreased significantly with the 1 µM dose only, while higher KAR_2 concentrations

bioRxiv preprint doi: https://doi.org/10.1101/2020.11.24.395954; this version posted November 24, 2020. The copyright holder for this preprint (which was not certified by peer review) is the author/funder. All rights reserved. No reuse allowed without permission.

(10 µM) had no significant effect (Supplemental Figure 1). KAR_2 application also reduced *caulonema* length in the *Ppccd8* mutant but at low concentrations (0.1 µM and 1 µM, Supplemental Figure 1). To conclude, KAR_2 phenotypic effects on *P. patens* were slight and not clearly dose responsive, similar to those of (–)-GR24.

We also tested racemic carlactone (CL), described as the natural product of PpCCD8 in *P. patens* (Decker et al. 2017). CL application had a negative effect on *caulonema* filament number for both WT and the *Ppccd8* mutant, however the effect was only significant at 10 µM in this case (Figure 2C).

Overall the findings from these phenotypic assays, suggest that GR24 enantiomers have distinct effects in *P. patens*, as observed in Arabidopsis (Scaffidi et al. 2014). Indeed, the (+)-GR24 analog mimics CL effects, although it is far more potent, and can thus be used to mimic the effects of PpCCD8-derived compounds. On the other hand, the (–)-GR24 analog has slight phenotypic effects, that resemble those of the KAR_2 molecule.

All *PpKAI2L* genes are expressed at relatively low levels and putatively encode proteins with a conserved catalytic triad

Figure 3 shows the predicted phylogenetic tree (Figure 3A) and the structure (Figure 3B) of all 13 *PpKAI2L* genes, along with that of *AtD14* and *AtKAI2*. A catalytic triad (Ser, His, Asp) is found in all genes (Supplemental Figure 2, alignment), including *PpKAI2L- A* and *M* for which recent sequencing data (P. patens v3.3, (Lang et al. 2008)) contradicts previous pseudogene predictions. In the following, the four subclades (previously described in (Lopez-Obando et al. 2016a), will be renamed for convenience: clade (A-E) for clade (i) including PpKAI2L-A, -B, -C, -D, and -E, clade (FK) for clade (ii) including PpKAI2L-F and -K, clade (HIL) for clade (i.i-i.ii) including PpKAI2L-H, -I, -L, and clade (JGM) for clade (iii) including PpKAI2L-J, -G, and -M.

We obtained the expression pattern of all *PpKAI2L* genes in *P. patens*, using a cDNA library from various organs/tissues (Supplemental Figure 3 A), including spores, *protonema* of increasing age and different tissue composition (6-day-old: primarily *chloronema*; 11-day-old: mix of *chloronema* and *caulonema*; 15-day-old: mix of *chloronema*, *caulonema* and gametophores buds), and gametophores from 5-week-old plants. *PpKAI2L* genes transcripts were detected in all tested tissues, at relatively low levels compared to the control genes. Notably, we also found that *PpKAI2L-A* is expressed, thus confirming it is not a pseudogene. Quantitative -PCR could not be used to assess expression of *PpKAI2L-M*, as its predicted

bioRxiv preprint doi: https://doi.org/10.1101/2020.11.24.395954; this version posted November 24, 2020. The copyright holder for this preprint (which was not certified by peer review) is the author/funder. All rights reserved. No reuse allowed without permission.

transcript is almost identical to that of *PpKAI2L-G*, and the observed transcript levels are attributable to both *PpKAI2L-G* and *-M*. Thus *PpKAI2L-G/M* probably arose recently as a local duplication in the *P. patens* genome. In spores, *PpKAI2L-F* and *-J* had higher transcript levels than other *PpKAI2L* genes. In *protonema* and gametophores however, *PpKAI2L-D* from clade (A-E) showed the highest transcript levels compared to any other *PpKAI2L* genes. *PpKAI2L-I* transcript levels are the lowest, in all tested tissues. When considering the clades separately (Supplemental Figure 3B-E), *PpKAI2L-D* had higher transcript levels among clade (A-E) genes, while *PpKAI2L-H* transcript levels were the highest compared to that of *PpKAI2L-I* and *-L* (clade (HIL)). *PpKAI2L-F* and *-K* (clade (FK)) showed comparable transcript levels, and *PpKAI2L-J* has slightly higher transcript levels than *PpKAI2L-G/M* (clade (JGM)). The data are consistent with those previously reported (Ortiz-Ramirez et al. 2016), shown in Supplemental Figure 4.

The PpKAI2L-C, -D, -E proteins are destabilized by (–)-GR24 as observed for AtKAI2; PpKAI2L-F, -K, -L and -H interact weakly with GR24 enantiomers

To investigate whether the PpKAI2L proteins behave similarly to AtD14 or AtKAI2 *in vitro*, seven PpKAI2L (-C,-D,-E,-F,-H,-K and -L) protein CDS were cloned for over-expression in *E. coli*, and successfully purified, in order to test their stability, interaction with SL analogs and potential enzymatic activities. Unfortunately, because of low solubility, none of the six other PpKAI2L proteins, especially from the clade (JGM) PpKAI2L could be purified in sufficient amounts to perform quality controls.

To test the interactions of purified PpKAI2L proteins with SL analogs, we used both nano Differential Scanning Fluorimetry (nanoDSF) (Figure 4) and classical DSF (Supplemental Figure 5). All four GR24 isomers destabilized AtD14, with the (+)-2'-*epi* enantiomer being the least potent inducer of destabilization (Figure 4B and Supplemental Figure 5B). The AtKAI2 Tm decreased following (–)-GR24 addition, indicating that it is destabilized by (–)-GR24 (Figure 4C and Supplemental Figure 5A), as previously reported (Waters et al. 2015a). All tested clade (A-E) proteins (PpKAI2L-C -D and -E) were destabilized when (–)-GR24 was added, as was AtKAI2 (Figure 4D-F and Supplemental Figure 5C-E). Puzzingly, the PpKAI2L-C, -D and -E proteins showed a tendency to be stabilized by (+)-GR24 at high concentrations (Supplemental Figure 5C-E). The other PpKAI2L proteins all showed different DSF profiles. Only the PpKAI2L-K (clade (FK)) was destabilized by both (–)-GR24 and (+)-

bioRxiv preprint doi: https://doi.org/10.1101/2020.11.24.395954; this version posted November 24, 2020. The copyright holder for this preprint (which was not certified by peer review) is the author/funder. All rights reserved. No reuse allowed without permission.

GR24, and stabilized by (+)-2'-*epi*-GR24 (Tm + 1.6 °C) (Figure 4H). PpKAI2L-L (clade (HIL)) showed a slight increase in Tm following addition of all four isomers (≤ 1°C), suggesting a slight stabilization (Figure 4J), that was not observed in a previous study (Bürger et al. 2019). None of the four isomers affected the stability of the PpKAI2L-F (clade (FK)) and PpKAI2L-H (clade (HIL)) proteins (Figure 4G,I and Supplemental Figure 5F-G).

The binding affinity of the PpKAI2L proteins for the GR24 isomers was further quantified using K_d affinity calculations following intrinsic tryptophan fluorescence measurements (Figure 5 and Supplemental Figure 6). Both PpKAI2L-D and PpKAI2L-E showed a comparable affinity for (–)-GR24, (respectively 92 µM and 39 µM), similar to that recorded for AtKAI2 (45 µM) and for AtD14 (94 µM) (Figure 5A-D). The K_d value for (+)-GR24 could not be determined due to the low affinity of these two proteins. While no change in PpKAI2L-H protein stability was observed in nanoDSF, interactions between this protein and all three GR24 stereoisomers ((–)-GR24 , (+)-GR24 and (–)-2'-*epi*-GR24) were detected (Figure 5G). K_d values between 100 µM and 200µM were estimated, indicating a weak affinity for these compounds. Finally, intrinsic flurorescence assays with PpKAI2L-F and PpKAI2L-K confirmed that these two proteins behave differently: PpKAI2L-F does not appear to interact with any GR24 stereoisomers, whereas PpKAI2L-K shows an affinity of 41 µM for (–)-GR24 and 107 µM for (+)-GR24 (Figure 5E-F).

Overall, all proteins from clade (A-E) show a similar biochemical behavior towards SL analogs, with a stereoselectivity for (–)-GR24, similar to AtKAI2. As to the proteins from the other tested clades, (HIL) and (FK), no specific features can be highlighted, indicating that these proteins need to be considered independently regarding their interaction with the ligand. Furthermore, these results show that PpKAI2L proteins from different clades can bind (+)-GR24 and (–)-GR24 stereosisomers, but this does not always have the same effect in terms of stability.

PpKAI2L-C, -D, -E, and -K preferentially cleave (–)-GR24, while PpKAI2L-H and -L cleave all four GR24 enantiomers

As most PpKAI2L proteins were able to bind at least one of the GR24 enantiomers, and since the catalytic triad is conserved in all of them, the next step was to test their enzymatic activity against SL analogs. When incubated with the generic substrate for esterases, 4-nitrophenyl

bioRxiv preprint doi: https://doi.org/10.1101/2020.11.24.395954; this version posted November 24, 2020. The copyright holder for this preprint (which was not certified by peer review) is the author/funder. All rights reserved. No reuse allowed without permission.

acetate (*p*-NPA), AtKAI2 and all tested PpKAI2L proteins showed enzyme activity (Supplemental Figure 7A-B). Kinetic constants were in the same range for all proteins, and similar to that of AtKAI2. The exception was PpKAI2L-H, which had a higher V_{max} and K_M, highlighting faster catalysis and a better affinity for *p*-NPA than all the others (Supplemental Figure 7C). The enzymatic activity of the PpKAI2L proteins was then tested against the four GR24 isomers, and compared to that of the pea SL receptor, RMS3/PsD14, and AtKAI2 (Figure 6A). All three PpKAI2L-C -D and -E (clade (A-E)) showed comparable enzymatic stereoselectivity towards GR24 isomers (between 15 and 20%), close, though significantly lower, to that of AtKAI2 that reached 30%. In contrast to AtKAI2, PpKAI2L-C -D and -E could also cleave the other isomers, nevertheless at to a lesser extent (5-10%) suggesting a less stringent selectivity. As for PpKAI2L proteins from clade (FK), PpKAI2L-F showed very low activity towards all four isomers (less than 5%), while PpKAI2L-K activity was comparable to that of clade (A-E) and to that of PpKAI2L-L (clade (HIL)). Finally, although none of the PpKAI2L proteins showed as high catalytic activity as RMS3 (100% cleavage of (+)-GR24, (–)-GR24 and (–)-2'-*epi*-GR24), the PpKAI2L-H protein showed a relatively high catalytic activity towards all four GR24 isomers, especially towards (–)-GR24 (almost 70%, Figure 6A).

The high enzyme activity of the PpKAI2L-H protein and lack of thermal shift when incubated with GR24 isomers suggests that this protein behaves differently to other PpKAI2L. To better characterize its enzyme activity, we used a pro-fluorescent probe as substrate ((±)-GC242), in which the ABC rings of GR24 are replaced by a coumarine-derived moiety (DiFMU) (de Saint Germain et al. 2016). (±)-GC242 is bioactive on moss as it reduced the number of *caulonema* filaments in the dark in a dose responsive manner (evaluated on the *Ppccd8* mutant, Supplemental Figure 8A). The use of (±)-GC242 as substrate confirmed that PpKAI2L-H has relatively high enzymatic activity, compared to all the other PpKAI2L proteins (Figure 6B). Indeed, after 2 hours, PpKAI2L-H catalyzed the formation of 1µM DiFMU, while other PpKAI2L activities were indistinguishable from background noise. However, the PpKAI2L-H enzymatic profile did not show the biphasic curve (a short burst phase, quickly followed by a plateau phase), which characterizes the AtD14 single turnover activity (Figure 6B, (de Saint Germain et al. 2016)). The lack of a plateau for PpKAI2L-H suggests that this protein acts as a Michaelian enzyme on SL analogs. To try to understand this singularity, we compared the solvent exposed residues in the binding pocket of the PpKAI2L proteins and noticed that PpKAI2L-H harbors a leucine[28] residue instead of the

bioRxiv preprint doi: https://doi.org/10.1101/2020.11.24.395954; this version posted November 24, 2020. The copyright holder for this preprint (which was not certified by peer review) is the author/funder. All rights reserved. No reuse allowed without permission.

phenylalanine found in AtD14 (F^{26}), AtKAI2 and all other PpKAI2L proteins (Figure 6C). The F residue is located at the junction between helix α4 and α5, near the catalytic site, and can precisely interact with the D-ring of the SL (Figure 6D). Furthermore, a mutant PpKAI2L-H protein where L^{28} is changed to F showed a biphasic cleavage profile similar to AtD14, both reaching a plateau at 0.4µM DiFMU, correlating with the protein concentration (Figure 6E-F). PpKAI2L-H and PpKAI2L-H^{L28F} proteins had comparable affinity towards (±)-GC242 ($K_{1/2}$= 4,794 µM *vs* 4,675 µM) but showed different *Vmax* values (V_{max}=0,06794 µM.min^{-1} *vs* 0,01465 µM.min^{-1}), suggesting that the L^{28} residue affects the velocity of catalytic activity. Thus, the PpKAI2L-H protein lacks a phenylalanine residue which partly explains its strong enzymatic activity.

Moss PpKAI2L proteins, like vascular plant receptors, covalently link GR24 enantiomers

To further investigate whether PpKAI2L proteins play a role as receptors, we examined covalent attachment of the GR24 isomers to the PpKAI2L proteins (Supplemental Figure 9). Mass spectrometry analyses highlighted 96 Da increments (corresponding to the D ring mass), when AtKAI2 was incubated with (–)-GR24, and all PpKAI2L-C, -D, -E, -F or -L were incubated with (–)-GR24. Strikingly, 96 Da increments were also observed when PpKAI2L-E -F -L and -K were incubated with the other isomer (+)-GR24. However, for PpKAI2L-E, the intensity peak was much lower with (+)-GR24 than with (–)-GR24, confirming the better affinity for the latter (Figure 5). PpKAI2L-H did not covalently bind the D ring, following incubation with either of both enantiomers, further suggesting that it displays Michaelien enzymatic activity and that this protein plays a specific enzymatic role. Poor interactions were observed with (+)-GR24, which was reported to mimick SLs, and had the most potent effect in our phenotypic assays (Figure 2 and Supplemental Figure 1). Strikingly, all clade (A-E) PpKAI2L proteins showed the strongest affinity for the (–)-GR24, reported in vascular plants as a good mimic for KL unknown compound (Scaffidi et al. 2014; Zheng et al. 2020).

Biochemical analysis of PpKAI2L proteins thus highlighted some resemblance to AtD14 and even more to the AtKAI2 protein, in accordance with a possible role as SL (or related compound) and/or KL receptors. *In planta* studies were then carried out to further investigate this possible role.

bioRxiv preprint doi: https://doi.org/10.1101/2020.11.24.395954; this version posted November 24, 2020. The copyright holder for this preprint (which was not certified by peer review) is the author/funder. All rights reserved. No reuse allowed without permission.

None of the *PpKAI2L* genes complement the Arabidopsis *d14-1 kai2-2* double mutant

We used cross species complementation assays to test whether any of the PpKAI2L proteins could carry out similar functions to that of AtD14 and/or AtKAI2 in Arabidopsis SL and/or KL signaling. The *PpKAI2L* (C, D, F, G, J, H) genes were cloned downstream of the AtD14 or AtKAI2 promoter, and the resulting constructs were expressed in the Arabidopsis double mutant At*d14-1 kai2-2*, which shows both a hyperbranched phenotype and elongated hypocotyls (Supplemental Figure 10A). As controls, the double mutant was transformed with the AtKAI2 or AtD14 CDS under the control of endogenous promoters. Only lines expressing AtD14 under the control of the AtD14 promoter fully restored rosette branching to WT (Ler) values (Figure 7A). Under the control of the AtD14 promoter, neither AtKAI2 or any of the PpKAI2L could significantly restore the branching phenotype of the At*d14-1 kai2-2* mutant, with the exception of one line expressing PpKAI2L-J (#4.6), which showed a significantly lower number of rosette branches than the mutant (still higher than WT or the AtD14 expressing line, Figure 7A). We conclude that none of the *PpKAI2L* genes can fully complement the function of AtD14 in shoot branching.

We also examined the possible complementation of the AtKAI2 function in the At*d14-1 kai2-2* mutant, by monitoring hypocotyl length under low light conditions, with or without 1 µM (+)-GR24 or (–)-GR24 in the culture medium (Figure 7 B). Compared to WT, the double mutant showed longer hypocotyls under control conditions, as did the single *kai2-2* mutant, and the addition of (+)-GR24 nor (–)-GR24 had no effect on this phenotype. In contrast, 1 µM (+)-GR24 in the medium led to shorter *kai2-2* hypocotyls, likely due to perception and transduction by the AtD14 protein which is still active in the single mutant. Accordingly, 1 µM (–)-GR24 in the medium had no effect on *kai2-2* hypocotyls. Expressing AtKAI2 under the control of the AtKAI2 promoter surprisingly did not fully restore the hypocotyl length of the double mutant under our control conditions, but it did restore the response to (–)-GR24 as expected. Even more surprisingly, the pKAI2:AtD14 expressing line showed longer hypocotyls than the double mutant under control conditions (DMSO). In addition, similar longer hypocotyl phenotypes were found under control conditions for lines expressing PpKAI2L-C (Supplemental Figure 10), PpKAI2L-J and PpKAI2L-H (Figure 7B). This unexpected effect of the introduced α/β hydrolases will be discussed below. In contrast, only lines expressing PpKAI2L-G had short hypocotyls under control conditions, suggesting that

bioRxiv preprint doi: https://doi.org/10.1101/2020.11.24.395954; this version posted November 24, 2020. The copyright holder for this preprint (which was not certified by peer review) is the author/funder. All rights reserved. No reuse allowed without permission.

the expressed protein had indeed complemented the AtKAI2 function. When either (+)-GR24 or (−)-GR24 was added, short hypocotyls (similar to WT) were observed in the pKAI2:AtD14 expressing line, indicating AtD14-mediated signal transduction of both enantiomers. However, adding GR24 enantiomers in the medium had no such effect on lines expressing PpKAI2L proteins (Figure 7B and Supplemental Figure 10), with the striking exception of lines expressing PpKAI2L-H, that showed a clear response to (+)-GR24 (shorter hypocotyls). Overall these assays showed that PpKAI2L-G is able to mediate Arabidopsis KL signaling in hypocotyls, even though it could not fully ensure the AtKAI2 response function; PpKAI2L-H appears to carry out a similar function to AtD14 in a *kai2-2* background, for hypocotyl development but not for rosette branching.

Multiplex editing of all *PpKAI2L* genes

Multiplex Gene Editing using CRISPR-Cas9 allows several genes to be knocked out in a single transformation experiment (Lopez-Obando et al. 2016b). Guide RNAs were chosen in each *PpKAI2L* gene, preferably in the first exon, to ideally obtain the earliest nonsense mutation possible. When no guide could be designed in the first exon, it was alternatively chosen to recognize a region in close proximity to the codon for one of the last two residues of the catalytic triad. (Figure 1B). The mutations obtained in each gene are described in Figure 8 and Supplemental Figure 11. Following DNA repair, small deletion (1-75 bp) and/or insertion-deletion events led to aa deletions, or a frame shift in the predicted protein sequence. We noted with an * the predicted knock out mutations due to premature STOP codons or a large deletion induced in the mutant sequences. The use of five guide RNAs simultaneously (Supplemental Table 1) allowed mutants affected in all of clade (A-E) genes to be isolated, as well as the generation of other mutants affected in fewer genes of this clade (see (Lopez-Obando et al. 2016b) and Supplemental Table 2). We chose two triple (*Ppkai2L-a2*-b4*-c2**, *Ppkai2L-c2*-d4*-e1)* and two quintuple mutants (*Ppkai2L-a1-b1-c1-d1-e2** *and Ppkai2L-a3*-b1-c3*-d3*-e2*)* for further analysis (Supplemental Table 2). The three other clades (HIL), (FK), and (JGM) were targeted in separate experiments using combinations of specific guide-RNAs for each gene. The same guide-RNA was used to target *PpKAI2L-G* and *-M*. Several mutants were obtained for clade (JGM) genes, including a single KO *Ppkai2L-j* mutant (*j1**) (Supplemental Table 2). As biochemistry experiments suggested a pure enzymatic role for PpKAI2L-H, a deletion mutant was obtained through homologous recombination, where the full CDS was removed from the moss genome (Δ*h* mutant, Figure 8

bioRxiv preprint doi: https://doi.org/10.1101/2020.11.24.395954; this version posted November 24, 2020. The copyright holder for this preprint (which was not certified by peer review) is the author/funder. All rights reserved. No reuse allowed without permission.

and Supplemental Figure 12A*)*. This Δ*h* mutant was chosen for further transformation experiments with guide-RNAs from the same (HIL) clade and/or from clade (FK) and (JGM), generating Δ*h-i-l and* Δ*h-f-k-j* mutants (Supplemental Table 2). Eventually, a 7X mutant was obtained (Δ*h-i-f-k-j-g-m)* where all the mutations except those in *PpKAI2L-J* and *-M* were null (Supplemental Table 2 and see below).

The *Ppkai2L* clade (A-E) quintuple mutants phenocopy *Ppmax2-1* in white light, while mutants in other clades are more similar to WT or *Ppccd8*

Our rationale was that a mutant affected in the response to PpCCD8-derived compounds should show a phenotype similar to that of the *Ppccd8* synthesis mutant. We first performed a phenotypic analysis of the mutants in light conditions. After four weeks of culture, *Ppccd8* mutant plants were slightly bigger than WT ((Proust et al. 2011), Figure 9), while the *Ppmax2-1* mutant was smaller, with fewer but bigger gametophores ((Lopez-Obando et al. 2018), Figure 9). The diameter of mutants in clade (A-E) genes was significantly smaller than that of *Ppccd8* and WT, and slightly larger than that of *Ppmax2-1* (Figure 9A-B and Supplemental Figure 12B). The phenotype of the clade (A-E) mutants, with early and large gametophores resembled that of the *Ppmax2-1* mutant although not as pronounced (Figure 9A). To the naked eye, three week-old plants from mutants of all three clades (FK) (JGM) and (HIL) genes were indistinguishable from WT (Figure 9A). These observations were also true for very young plants (10 day-old, Supplemental Figure 12B). After a month of growth however, all mutants affecting genes from clade (FK) and (JGM) showed a slightly larger diameter, intermediate between that of WT and *Ppccd8*. The triple *Ppkai2L j3-g3*-m1* mutant was even larger than *Ppccd8* (Figure 9C and D). Mutants in clade (HIL) such as *Ppkai2L* Δ*h*, *Ppkai2L* Δ*h-i2** and *Ppkai2L* Δ*h-i3*-l1* looked the same as WT (Figure 9D and Supplemental Figure 12B).

Like *Ppmax2* Clade (A-E) quintuple mutants are affected in photomorphogenesis

Mutants in clade (A-E) genes showed the typical phenotype of the *Ppmax2-1* mutant in white light. We previously showed that the *Ppmax2-1* mutant is affected in photomorphogenesis under red light (Lopez-Obando et al. 2018). After two months growing under red light, *Ppmax2-1* gametophores were much more elongated than WT gametophores, whereas *Ppccd8* mutant gametophores were shorter (Figure 10). Among clade (A-E) mutants, gametophores of both triple mutants *Ppkai2L a2*-b4*-c2** and *Ppkai2L c2*-d4*-e1* were a similar height to

bioRxiv preprint doi: https://doi.org/10.1101/2020.11.24.395954; this version posted November 24, 2020. The copyright holder for this preprint (which was not certified by peer review) is the author/funder. All rights reserved. No reuse allowed without permission.

WT. Interestingly, the quintuple mutant (*Ppkai2L a1-b1-c1-d1-e2**) showed significantly elongated gametophores, similar to *Ppmax2-1* (Figure 10 A and C). The other tested quintuple mutants (*Ppkai2L a3*-b1-c3*-d3*-e2** and *a1-b1-c1-d1-e2**) also had elongated gametophores under red light, intermediate between WT and *Ppmax2-1* (Supplemental Figure 13). The weak phenotype of both triple mutants suggests a functional redundancy among clade (A-E) genes, as KO mutations for PpKAI2L-A, B, C and/or D did not result in as elongated gametophores as in the *Ppmax2-1* mutant.

Gametophores from mutants where genes from clade (FK) and/or (JGM) were mutated (*Ppkai2L f2*-j5-k2**, *Ppkai2L* Δ*h-f1*-j4-k1** and Δ*h-f1*-j4-k1*-g2*-m1*, Figure 10B) were similar in height to WT, suggesting that genes from clade (FK) and clade (JGM) have no role in photomorphogenesis in red light. The clade (HIL) *Ppkai2L* Δ*h-i2**and *Ppkai2L* Δ*h-i3*-l1* mutants showed shorter gametophores under red light, similar to *Ppccd8* (Figure 10A, C., In contrast, the gametophores of the single *Ppkai2L* Δ*h* mutant were intermediate in height between WT and *Ppccd8* (Figure 10B). This may suggest a specific role for the (HIL) clade genes, opposed to that of *PpMAX2*, or unrelated to the PpMAX2 pathway.

In conclusion, the phenotype of the *Ppkai2L* mutants in red light allowed the functions of the clade (A-E) genes to be differentiated. These are likely to be involved in a PpMAX2 dependent pathway, related to photomorphogenesis, whereas genes from the three other clades (DDK clade), are more likely to be play a role independent from this pathway.

Mutants in the (JGM) clade no longer respond to (+)-GR24 application

In the assays reported above, we measured the response of WT and *Ppccd8* mutant to SLs analogs (Figure 2). To determine which of the *Ppkai2L* mutants may carry mutations in potential receptors for PpCCD8-compounds (SL-related) or other (KL-related) compounds, we tested their phenotypic response in the dark to GR24 enantiomer. We used a concentration of 0.1 µM in all assays and counted the number of *caulonema* filaments per plant.

For the (A-E) clade, under control conditions, all *Ppkai2L* mutants showed an equivalent number of filaments to WT. The exception was the quintuple mutant, which tended to have less filaments in control conditions, a smilar phenotype to *Ppmax2-1* (Figure 11A-B and Supplemental Figure14A). Addition of 0.1 µM (–)-GR24 did not have a significant effect on clade (A-E) mutants or WT (Figure 11A). However, in this assay, both the *Ppccd8* and *Ppmax2-1* mutants showed a significant decrease in *caulonema* filament number. In a

bioRxiv preprint doi: https://doi.org/10.1101/2020.11.24.395954; this version posted November 24, 2020. The copyright holder for this preprint (which was not certified by peer review) is the author/funder. All rights reserved. No reuse allowed without permission.

separate experiment, a dose of 1 µM of (–)-GR24 had opposite effects on *caulonema* WT and *Ppccd8* filament number with an increase and decrease, respectively (Supplemental Figure 14 A, and Figure 2 above), but had no significant effect on the *Ppmax2-1* mutant, although the same tendency towards a decrease was observed. At this higher dose, the quintuple mutant, affected in all five *PpKAI2L-A to E* genes, showed a significant decrease in *caulonema* filament number, like *Ppccd8,* but in contrast to WT. Thus, similar to *PpMAX2* loss of function, mutating clade (A-E) *PpKAI2L* genes does not abolish a response to the (–)-GR24 enantiomer. Application of (+)-GR24 had a significant negative effect on the number of filaments for the quintuple *Ppkai2L a3*-b1-c3*-d3*-e2** mutant, WT and the *Ppccd8* and *Ppmax2-1* mutants (Figure 11 B). Thus, mutating any of the clade (A-E) *PpKAI2L* genes does not hamper the response to (+)-GR24, and therefore likely the response to CCD8-derived compounds.

We then tested the effect of GR24 enantiomers on *Ppkai2L* mutants from the three other clades (Figure11 C-E and Supplemental Figure 14). Strikingly, under control conditions, like *Ppccd8,* all the mutants had more filaments than WT, except for clade (HIL) mutants which tended to have less filaments (Figureure 11C-E and Supplemental Figure14). Both the single mutant *Ppkai2L-j1** and the quintuple mutant *Ppkai2L j1*-g1-m6*-i3*-l2* showed a significant response to (–)-GR24 (less *caulonema*), as did *Ppccd8* (Figure 11C and Supplemental Figure 14 A,B). No clear response to (–)-GR24 was seen in mutants with KO mutations in *PpKAI2L-F, -K, -H, -G, -M, -I* or *-L* or WT.

When we examined the response to (+)-GR24 for mutants of the (FK) (JGM) and (HIL) clades (Figure11 D-E and Supplemental Figure 14 C,D), the number of *caulonema* was clearly reduced in WT and *Ppccd8,* and in mutants carrying the *Ppkai2L ⊿h* mutation, alone or in combination with *f**, *k* i** or *l** null mutations. Thus clade (FK) and clade (HIL) genes do not play a role in the response to (+)-GR24. However, the response to the (+)-GR24 enantiomer is abolished in all mutants where the *PpKAI2L-J* gene is KO (Figure11 D: *j1** and *j1*-g2*-m2**, and Supplemental Figure 14 C,D). Interestingly, in the two lines where the *j* mutation is not null but the *PpKAI2L-G* gene is KO (7x and *j6-g5*-m1* mutants), the response to (+)-GR24 was also abolished (Supplemental Figure14 C,D). Thus, from phenotypic assays on mutant *caulonema*, both the *PpKAI2L-J* and *-G* genes appear to be involved in the response to (+)-GR24, and are therefore the best candidates for receptors to PpCCD8-derived molecules.

bioRxiv preprint doi: https://doi.org/10.1101/2020.11.24.395954; this version posted November 24, 2020. The copyright holder for this preprint (which was not certified by peer review) is the author/funder. All rights reserved. No reuse allowed without permission.

To confirm that PpKAI2L-J and -G are likely receptors for PpCCD8-derived molecules, we measured the transcript levels of SL responsive genes in the corresponding mutants (Figure 12). We previously reported that in WT and the *Ppccd8* mutant, *PpKUF1LA* gene transcript abundance increases 6 h after plant transfer onto medium containing 3 µM (±)-GR24, and that this response is enhanced in dark conditions (Lopez-Obando et al. 2018). We used this marker along with the *Pp3c6_15020* gene, previously found to be upregulated by (±)-GR24 (our unpublished data). Using GR24 enantiomers, we confirmed that transcript levels for both genes increased following 1 µM (+)-GR24 addition in WT and *Ppccd8*, but not in *Ppmax2-1*. Strikingly, an increase in transcript levels following (–)-GR24 application was observed for both markers in the *Ppccd8* mutant, and for *PpKUF1LA* only in WT (Figure 12). In the quintuple mutant of clade (A-E), addition of (+)-GR24 but not (–)-GR24 increased *PpKUF1LA* and *Pp3c6_15020* transcript levels . In contrast, in the *Ppkai2L-j1** mutant, transcript levels of both genes increased following (–)-GR24 addition, and was slightly increased (*PpKUF1LA*) or unchanged (*Pp3c6_15020*) by (+)-GR24 application. In the *Ppkai2L j3-g3*-m1* mutant, the response marker transcript levels increased slightly (*PpKUF1LA*) or remained unchanged with (+)-GR24 addition, but were unchanged by (–)-GR24. Thus, the transcriptional response of the tested mutants confirms that clade (A-E) genes are not involved in the response to (+)-GR24, while this response is impaired in clade (JGM) mutants. Only the *Ppccd8* and *Ppkai2L-j1** mutants showed a clear and significant transcriptional response, with both markers, to (–)-GR24 addition.

DISCUSSION

Are PpCCD8-derived products non-canonical SLs?

PpCCD8-derived products are germination stimulants of *P. ramosa* group 2a seeds, harvested in a hemp field, but do not induce the germination of *P. ramosa* group 1 seeds, collected from an oilseed rape field. (Decker et al. 2017) also reported that *P. patens* exudates could induce the germination of *Orobanche ramosa* (old denomination of *Phelipanche ramosa*) seeds but without specifying the origin of the tested population. Differences in the suceptibility of root parasitic weeds can be attributed to the chemical nature of host plant exudates (Yoneyama et al. 2018b). Our results suggest that the PpCCD8-derived products share similarities with hemp secondary metabolites. So far, no known canonical SLs has been isolated from hemp (Huet et al. 2020). Since *P. patens* likely produces carlactone (Decker et

bioRxiv preprint doi: https://doi.org/10.1101/2020.11.24.395954; this version posted November 24, 2020. The copyright holder for this preprint (which was not certified by peer review) is the author/funder. All rights reserved. No reuse allowed without permission.

al. 2017), but lacks a true *MAX1* homolog (Proust et al. 2011), we can hypothesize that PpCCD8-derived compounds correspond to non-canonical SLs, derived from carlactone or hydroxyl carlactones (Yoneyama 2020). Indeed, among analogs showing bioactivity on *P. patens caulonema* length, we previously showed that GR5, a non-canonical analog, was as active as (±)-GR24 (Hoffmann et al. 2014). As mimics of SLs in the present study, we used the (+)- and (–)-GR24 artificial analogs, available at the time of our study (see below). Of note, both isomers are active on *P. ramosa* group 1 and group 2a seeds. However, the (+)-GR24 isomer, which has a canonical SL structure, has similar germination stimulating activity to (±)-GR24, while the (–)-GR24 isomer is far less active (de Saint Germain et al. 2019). For future identification of PpCCD8-derived compounds, non-canonical SL analogs such as the recently described Methyl Phenlactonoates (Jamil et al. 2020) may be more appropriate.

Looking for the best mimic of SLs or KL

The (–)-GR24 analog has a non-natural configuration, meaning a configuration that has never been isolated from plant exudates, contrary to the (+)-GR24 enantiomer, that bears similarity to 5-deoxystrigol ((+)-5DS) and strigol-type canonical SLs (Scaffidi et al. 2014). In our bioassays of moss phenotypes, CL application decreased the number of *caulonema* of both WT and the *P. patens* mutant, in a dose-responsive manner. A similar (but much stronger) effect was observed with (+)-GR24, that we thus consider as the best mimic of *P. patens* CCD8-derived compounds. It is not surprising that (+)-GR24 is more potent than CL, as assays were carried out in a wet medium and natural SLs were described as being far less stable than synthetic analogs in aqueous medium (Akiyama et al. 2010; Boyer et al. 2012). In contrast, the effects of (–)-GR24 are weak, not dose responsive, and sometimes contradictory in WT versus the *Ppccd8* mutant. Indeed, in several assays, we observed a significant increase in *caulonema* number in WT (Figure 2, Supplemental Figure 14A) while this number consistently decreased in *Ppccd8* (Figure 11, Supplemental Figure 14 A, B). Interestingly, we also observed an increase in *caulonema* number when testing KAR_2, although this increase was only significant at 10 µM for *Ppccd8*. So far we had not observed any effect of karrikins (KAR_1) on *P. patens* phenotypes (Hoffmann et al. 2014), and this is thus the first hint of a possible effect of some karrikins on moss, which needs to be confirmed. It is puzzling however that the effect of KAR_2 is better seen in *Ppccd8* (thus in the absence of SLs), while the effect of (–)-GR24 is better seen in WT compared to *Ppccd8*. We propose (Figure 13 and see below) that clade (JGM) PpKAI2L proteins possibly perceive (–)-GR24, which would

bioRxiv preprint doi: https://doi.org/10.1101/2020.11.24.395954; this version posted November 24, 2020. The copyright holder for this preprint (which was not certified by peer review) is the author/funder. All rights reserved. No reuse allowed without permission.

explain the apparent contrary effects of this enantiomer observed in WT and *Ppccd8*. Thus, (−)-GR24 is not a very robust mimic of the as yet unidentified moss KL. This could also suggest that the moss KL may be quite different from that of angiosperms.

Biochemical characterization of the PpKAI2L proteins highlights that those from the (A-E) subclade may act as KL receptors

In biochemistry experiments, among the analogs used, we observed the best binding of the (−)-GR24 enantiomer to AtKAI2 and all tested PpKAI2L proteins from the (A-E) clade. This confirms a recent report (Bürger et al. 2019) of preferential binding of (−)-5DS by PpKAI2L-C, -D and -E. Surprisingly, (+)-GR24 interacts poorly with these PpKAI2L proteins. As the (−)-GR24 enantiomer is a KL mimic in Arabidopsis, this result suggests that clade (A-E) PpKAI2L proteins share a perception mechanism with AtKAI2, and furthermore may recognize KL-like compounds. It should be noted that AtKAI2 is degraded following KAR perception, in a MAX2-independent manner (Waters et al. 2015a), and this could be tested on clade (A-E) PpKAI2L proteins. As with the two other tested clades (FK) and (HIL), none of the interaction assays highlighted any preferential binding of GR24 enantiomers. Unfortunately, none of the PpKAI2L proteins from clade (JGM) could be purified for interaction assays, which was also reported by (Bürger et al. 2019). In the future, overexpression in *P. patens* or in other heterologous systems (yeast, insect cells) may be a solution for producing these proteins and carrying out biochemistry studies.

PpKAI2L-H is the most efficient hydrolase among PpKAI2L proteins

The PpKAI2L-H protein shows strong cleavage activity towards all four GR24 stereoisomers as well as towards the synthetic probe (±)-GC242, compared to any other PpKAI2L protein, but also compared to the Arabidopsis AtKAI2 and AtD14 proteins. Mutating the Leu^{28} residue into a Phe is sufficient to reduce the efficiency of this activity (strong reduction of the k_{cat} and of the V_{max}), but has no effect on the $K_{1/2}$ towards (±)-GC242. The efficient cleavage activity of PpKAI2L-H is therefore not likely due to a stronger affinity of this protein for the substrate. This is in accordance with the previous hypothesis that the Leu^{28} residue (as the Phe^{181} residue), that is unique to PpKAI2L-H, does not particularly enlarge the pocket size of PpKAI2L-H (Bürger et al. 2019). Furthermore, our results may highlight the ability of a

bioRxiv preprint doi: https://doi.org/10.1101/2020.11.24.395954; this version posted November 24, 2020. The copyright holder for this preprint (which was not certified by peer review) is the author/funder. All rights reserved. No reuse allowed without permission.

residue to control exit of the cleavage reaction product. Indeed, the conserved Phe[28] residue in D14/KAI2 proteins may act as gate keeper and this could explain the single turnover kinetics observed with some SL analogs (de Saint Germain et al. 2016). Among other plant D14/KAI2 proteins, hydrolytic activity is observed for the pea PsD14/RMS3 towards three out of four GR24 enantiomers (this study, Figure 6A), and has also been reported for two KAI2 homologs, from *Selaginella moellendorffii* (SmKAI2b, towards (+)-GR24) and *Marchantia polymorpha* (MpKai2b, towards (–)-GR24 (Waters et al. 2015b)). The conserved strong enzymatic activity of PpKAI2L-H would thus have a specific (and ancient) role in plants, perhaps as a cleaning enzyme, to eliminate an excess of signaling molecules (Seto et al. 2019).

When only the *PpKAI2L-H* gene is mutated (Δ*h* mutant), no striking phenotype is observed (Supplemental Figure 12B), and in particular, the phenotypic response to (+)-GR24, that mimics CCD8-derived compounds, is similar to that of WT plants (Figure 11D), in contrast to the other mutants (see below). In red light however, the gametophores of Δ*h-i2* and* Δ*h-i3*-l1* mutants are less elongated than WT gametophores, which is also observed in *Ppccd8*. However, in *Ppccd8* this could be related to the higher number of filaments, leading to the initiation of more (but smaller) gametophores, whereas the number of filaments in the dark is not higher in clade (HIL) mutants. In addition, clade (HIL) mutants tend to have less filaments than WT (Figure 11D, E and Supplemental Figure 14A). Altogether, although quite tenuous, these phenotypes could suggest that clade (HIL) genes undertake a specific role in *P. patens* development. The association of this role with PpKAI2L-H enzymatic activity remains to be discovered.

The Arabidopsis At*d14-1 kai2-2* mutant complementation assay is more than anecdotal

Using the endogenous AtD14 promoter, we confirmed that expression of the PpKAI2L-C and H proteins does not complement the Arabidopsis D14 function in rosette branching, as previously reported using the 35S promoter (Bürger et al. 2019). We can extend this observation to PpKAI2L-D, PpKAI2L-F and PpKAI2L-G, which were never previously tested for rosette branching complementation. Interestingly, one line expressing PpKAI2L-J did show partial complementation of branching that could be a hint of a SL perception function for this protein. However, given the phenotype of *P. patens* mutants in clade (JGM), PpKAI2L-G expressing lines would have also been expected to complement the branching

bioRxiv preprint doi: https://doi.org/10.1101/2020.11.24.395954; this version posted November 24, 2020. The copyright holder for this preprint (which was not certified by peer review) is the author/funder. All rights reserved. No reuse allowed without permission.

phenotype, unless the PpKAI2L-J is more active than its counterparts from the same clade. Using the endogenous AtKAI2 promoter, we also confimed as observed by (Bürger et al. 2019), that PpKAI2L-C and -H cannot complement the *kai2-2* mutation, and that this observation is extended to PpKAI2L-D, and -J. However, expressing moss PpKAI2L-G reduces the size of At*d14-1 kai2-2* hypocotyls, suggesting that PpKAI2L-G may be able to perceive and transduce the endogenous KL signal, even though it does not to respond to (–)-GR24. Strikingly, when expressed under the control of AtKAI2 promoter in the Arabidopsis At*d14-1 kai2-2* mutant, the AtD14 protein but also the moss PpKAI2L-C, -J or -H proteins exacerbates the defect induced by the *kai2-2* mutation by leading to even more elongated hypocotyls. This suggests a putative interaction of these proteins with the Arabidopsis KAI2/KL pathway that should be further investigated. Even more strikingly, (+)-GR24-induced shorter hypocotyls are observed in PpKAI2L-H expressing lines, as in AtD14 expressing lines, which may indicate that the strong hydrolytic activity of PpKAI2L-H can fulfil AtD14 function in the seedling. Still, it is clear that none of the PpKAI2L proteins fully complements the AtD14 or KAI2 function.

Genetic analysis suggests that genes from the (A-E) clade are involved in the PpMAX2 dependent pathway

Mutant phenotypes clearly distinguish clade (A-E) from the three other clades. Indeed, the quintuple PpKAI2L-A to -E mutant shows a phenotype in white light quite similar to that of *Ppmax2-1*. It also has elongated gametophores under red light, and a low number of *caulonema* filaments in the dark, suggesting that clade (A-E) PpKAI2L and PpMAX2 proteins could be members of the same pathway (Figure 13). As PpKAI2L proteins from the (A-E) clade preferentially bind the (–)-GR24 enantiomer, we expected the mutants in this clade to be blind to (–)-GR24 application. This is what we observed when transcriptional response markers were examined, with transcript levels remaining unchanged following (–)-GR24 application in both the *Ppmax2-1* and the quintuple (clade A-E) *Ppkai2l* mutant, but increasing in the *Ppccd8* mutant (but not in WT, Figure 12). However, as mentioned above, (–)-GR24 does not appear to be a good mimic of the unknown moss KL, and other transcriptional response markers need to be found, that would better reflect the moss KL response. As for the phenotypic response, application of 0.1 µM (–)-GR24 had no effect on clade (A-E) mutant *caulonema* number in the dark, or on WT, but significantly decreased

bioRxiv preprint doi: https://doi.org/10.1101/2020.11.24.395954; this version posted November 24, 2020. The copyright holder for this preprint (which was not certified by peer review) is the author/funder. All rights reserved. No reuse allowed without permission.

both *Ppccd8* and *Ppmax2-1 caulonema* number (Figure 11A). Strikingly, a 1 µM concentration of (–)-GR24, that has the opposite effect on WT (increases *caulonema* number) and *Ppccd8* (decreases *caulonema* number), led to no response in the *Ppmax2-1* mutant, while the quintuple (clade A-E) mutant showed a significant decrease in *caulonema* number (Supplemental Figure 14). Thus the quintuple (clade A-E) mutant is still able to perceive (–)-GR24, as well as the *Ppmax2-1* mutant. This does not rule out the hypothesis that clade (A-E) PpKAI2L and PpMAX2 proteins are in a same pathway, but further indicates that the (–)-GR24 enantiomer is a poor mimic of a moss KL. In addition, (–)-GR24 was reported to have a dual effect, promoting both the KAI2 and the D14 pathways in Arabidopsis roots (Villaecija-Aguilar et al. 2019), and this could explain the residual response of the clade (A-E) *Ppkai2l* mutant, through other PpKAI2L proteins, in a PpMAX2 independent pathway (see Figure 13 and below).

Finally, both phenotypic response in the dark and transcriptional response to the (+)-GR24 enantiomer are unaffected in the clade (A-E) *Ppkai2l* mutant, suggesting that clade (A-E) PpKAI2L proteins are not receptors for CCD8-derived compounds.

PpKAI2L- J, -G, -M mediate PpCCD8-derived (SL-related) responses

In white light conditions (Figure 9), mutants affecting clades other than (A-E) show phenotypes either similar to WT (mutants in clade (HIL) genes), or intermediate between WT and *Ppccd8* (mutants in clade (FK) and (JGM) clades). In the dark in control conditions (Figure 11), the *caulonema* number of mutants in clades (FK) and (JGM) is also intermediate between that of WT and *Ppccd8* , while it is similar to WT (or slightly smaller) in clade (HIL) mutants. Based on the hypothesis that synthesis and response mutants show similar phenotypes, genes from clades (FK) and (JGM) are thus the best candidates for PpCCD8-derived compound receptors. When the phenotypic response of these mutants to (+)-GR24 application was examined, plants with KO mutations in *PpKAI2L-J* or *PpKAI2L-G/M* (Figure 11, *j1**, and *j1*-g2*-m2**, and Supplemental Figure 14, *j7*-g1–m1*, *j8*-g1 –m5**, and *j6-g5*–m1*) no longer responded to this compound. In contrast, both *Δh-f1*-k1*-j4 and Δh-f3*-k3*-j6* mutants, show a significant response to (+)-GR24 application (Figure 11 and Supplemental Figure 14), indicating that KO mutations in both *PpKAI2L-F* and *PpKAI2L-K*, or deletion of *PpKAI2L-H* do not abolish the response to the CCD8-derived mimic compounds, not even additively. The absence of a response in higher order mutants where either *PpKAI2L-J* or *PpKAI2L-G* are KO confirms the prominent role of both genes in the

bioRxiv preprint doi: https://doi.org/10.1101/2020.11.24.395954; this version posted November 24, 2020. The copyright holder for this preprint (which was not certified by peer review) is the author/funder. All rights reserved. No reuse allowed without permission.

response to (+)-GR24. However, if, as expected, transcript levels of the *Pp3c6_15020* response marker gene did not change in either *j1** and *j3-g3*-m1* mutants following (+)-GR24 application (Figure 12), transcript levels of the *PpKUF1LA* gene increased in both mutants, suggesting a response to the SL analog. Thus, while the KO mutation of either *PpKAI2L-J* or *PpKAI2L-G* is sufficient to abolish the phenotypic response in the dark, it does not completely abolish the transcriptional response to (+)-GR24. Presumably, mutation of both *PpKAI2L-J* and *-G* or even all three genes (*-J-G-M*) is necessary to fully impair this response. Another possibility is that the transcriptional markers, first identified using (±)-GR24 (Lopez-Obando et al. 2016a; Lopez-Obando et al. 2018) are not fully specific for assaying the response to enantiomers. This result could also suggest that the transcriptional response, which is assessed far earlier than the phenotypic response (6 hours versus 15 days), is perhaps more sensitive to a very slight activation of the CCD8-derived compound pathway by PpKAI2L proteins.

PpKAI2L proteins are likely receptors in two separate pathways, one which is dependent and one which is independent from the PpMAX2 F-box protein.

Our previous results on the PpMAX2 F-box protein indicated that, in contrast to its homolog in flowering plants, it is not involved in the response to CCD8-derived compounds (Lopez-Obando et al. 2018). Like MAX2 in flowering plants however, PpMAX2 plays a role in early gametophore development and photomorphogenesis. We suggested that PpMAX2 could play a role in the moss KL signalling pathway, but we lacked evidence for other actors in this pathway in *P. patens*. The present study suggests that PpKAI2L-A to -E are α/β hydrolases involved in the same pathway as PpMAX2, since mutating these genes resulted in similar light-related phenotypes as those of the *Ppmax2* mutant. Specific mimics for the moss KL are however still missing for further evidence that PpKAI2L-A-E are receptors of the moss KL (Figure 13). Still, these results are consistent with the view that the KL pathway is ancestral relative to the SL pathway, and that the ancestral role of MAX2 in the land plants lineage is the transduction of the KL signal (Bythell-Douglas et al. 2017; Walker et al. 2019). Such a KL pathway has been very recently reported in *M. polymorpha*, further supporting this view (Mizuno et al. 2020).

PpKAI2L-J and PpKAI2L-G proteins are likely receptors of CCD8-compounds, which we suspect to be non-canonical SLs. Strikingly, these receptors are not particularly more similar to D14 than other PpKAI2L proteins. As hypothesized earlier (Lopez-Obando et al. 2016a;

bioRxiv preprint doi: https://doi.org/10.1101/2020.11.24.395954; this version posted November 24, 2020. The copyright holder for this preprint (which was not certified by peer review) is the author/funder. All rights reserved. No reuse allowed without permission.

Bythell-Douglas et al. 2017), the expansion of the PpKAI2L family in *P. patens* (and not in other bryophytes such as *Marchantia polymorpha*, that contains two *MpKAI2* genes), as in parasitic angiosperms (Conn et al. 2015; Toh et al. 2015), may have allowed the emergence of SL sensitivity (de Saint Germain et al. 2020). Neofunctionalization of additional KAI2 copies in *P. patens* ancestry towards SL perception is therefore a possible explanation for our findings in this moss and would reveal a convergent evolution process, relative to the emergence of D14 in seed plants. We can also imagine that these neofunctionalized PpKAI2L lost the ability to interact with MAX2 in *P. patens*, and established a different protein network that potentially integrates new factors such as an alternative F-box. The remaining question is therefore to determine how clade (JGM) PpKAI2L proteins are involved in transducing the SL signal downstream of perception.

Consequently, the search for proteins that interact with *P. patens* KL and CCD8-derived compound receptors should be a priority in the near future. In particular, since SMXL proteins are key members of both the SL and KL pathways in flowering plants (Soudappan et al, 2015, 2017; Wang et al, 2015; Khosla et al, 2020), specific involvement of PpSMXL homologs (four genes) is currently under investigation.

Five more PpKAI2L proteins are present and expressed in *P. patens* (Lopez-Obando et al, 2016), and mutant analyses indicate that those are neither KL nor CCD8-derived compound receptors. Three of them however, among which the efficient hydrolase PpKAI2L-H, are likely involved in *P. patens* development, through pathways that remain to be discovered.

METHODS

Plant Materials and Growth Conditions

The *Physcomitrium* (*Physcomitrella*) *patens* Gransden wild-type (WT) strain was used and grown as previously described (Hoffmann et al. 2014; Lopez-Obando et al. 2018) in long day (16h) conditions. Unless otherwise stated in legends, experiments were always carried out on $PpNO_3$ medium (minimal medium described by Ashton et al., 1979), in the following control conditions: 25°C during the day and 23°C at night, 50% humidity, quantum irradiance of ~80 µmol/m^2/s. Tissues from young *protonema* fragments were multiplied prior to every experiment in the same conditions but using medium with higher nitrogen content ($PpNH_4$ medium, $PpNO_3$ medium supplemented with 2.7 mM NH_4 tartrate). For red light experiments,

bioRxiv preprint doi: https://doi.org/10.1101/2020.11.24.395954; this version posted November 24, 2020. The copyright holder for this preprint (which was not certified by peer review) is the author/funder. All rights reserved. No reuse allowed without permission.

plants were grown on $PpNO_3$ medium in Magenta pots at 25°C, in continuous red-light (~45 µmol µmol/m^2/s).

Germination assays on root parasitic plant seeds

P. patens WT plants were grown on $PpNH_4$ plates with cellophane disks for two weeks then the plants (and cellophane) were transferred onto $PpNO_3$ medium with low phosphate (Phosphate buffer was replaced with 1g/L of MES buffer and the pH adjusted to 5.8) for another two weeks. *P. patens* exudates were collected by transferring the plants (still on cellophane disks) onto plates containing 10 mL distilled water and incubating them in the growth chamber with gentle agitation. After 48h, exudates were pipeted and filtered (0.2 µm). Exudates were diluted twice prior to testing their germination stimulating activity on preconditioned seeds of parasitic plants, as described previously (Pouvreau et al. 2013). Distilled water was used as a control. For germination assays on plates (Figure 1B-C), WT and the *Ppccd8* mutant were cultivated as above, and *P. ramosa* seeds were placed onto the plates after 10 days of phosphate starvation. Seeds were counted on three plates, with 7-10 microscope fields per plate.

CRISPR-Cas9 mediated mutagenesis and homologous recombination

P. patens mutants were obtained as described in (Lopez-Obando et al. 2016b), using CRISPR-Cas9 technology. *PpKAI2L* coding sequences were used to search for CRISPR RNA (crRNA) contiguous to a PAM motif recognized by *Streptococcus pyogenes* Cas9 (NGG), using the webtool CRISPOR V4 against the *P. patens* genome Phytozome V9 (http://crispor.tefor.net/). crRNAs located in the first third of the coding sequence, with the highest possible specificity scores, and fewest possible predicted off-targets, were selected. Small constructs containing each crRNA fused to either the proU6 or the proU3 snRNA promoters (Collonnier et al. 2017) between the attB1/attB2 Gateway recombination sequences, were synthesized by Twist Biosciences. These inserts were then cloned into pDONR207 vectors (Invitrogen). Polyethylene glycol–mediated protoplast transformation was performed with multiple pDONR207-sgRNA according to the protocol described by Lopez-Obando et al., 2016.

bioRxiv preprint doi: https://doi.org/10.1101/2020.11.24.395954; this version posted November 24, 2020. The copyright holder for this preprint (which was not certified by peer review) is the author/funder. All rights reserved. No reuse allowed without permission.

Mutations in the *PpKAI2L* genes were confirmed by PCR amplification of *PpKAI2L* loci around the recognition sequence of each guide RNA, and sequencing of the PCR products.

The PpKAI2L-H (Δ*h*) deletion mutant was obtained through homologous recombination. The full coding sequence of PpKAI2L-H from the ATG to stop was replaced with a resistance cassette. A 550 bp *PpKAI2L-H* 5' CDS flanking sequence was cloned into the pBNRF vector (Thelander et al. 2007) cut with BstBI/XhoI. Then a 500 bp *PpKAI2L-H* 3' CDS flanking sequence was cloned into the BNRF-*PpKAI2L-H* 5' construct digested with BcuI, so that the kanamycin resistance cassette of the vector was flanked by the PpKAI2L-H 5' and 3' sequences. *P. patens* WT protoplasts were transformed with the resulting construct as described previously (Lopez-Obando et al. 2016b) and transformants selected on 50mg/L Geneticin/G418. Transient expression of the CRE recombinase (Trouiller et al. 2006) in a confirmed transformant removed the resistance cassette to obtain the *Ppkai2l*-Δ*h* mutant, as described Figure 8 and Supplemental Figure 12.

Phenotypic assays on *P. patens*

Analysis of *caulonema* growth in the dark was performed in 24-well plates, starting from very small pieces of protonema. These were grown for ~ two weeks in control conditions before being placed vertically and incubated (± treatment) in the dark for ~10 days. A single picture of each well was taken using an axiozoom (Zeiss) with a dedicated program. *Caulonema* were counted and measured using ImageJ (http://imagej.nih.gov/ij/) (see also (Guillory and Bonhomme 2021)).

Chemicals

Racemic and pure enantiomers of GR24 and the (±)-GC242 probe were produced by F-D Boyer (ICSN, France). Racemic CL was kindly provided by A. Scaffidi (University of Western Australia, Perth, Australia). Chemicals were diluted in DMSO or acetone as indicated in figure legends.

RT-qPCR analysis

bioRxiv preprint doi: https://doi.org/10.1101/2020.11.24.395954; this version posted November 24, 2020. The copyright holder for this preprint (which was not certified by peer review) is the author/funder. All rights reserved. No reuse allowed without permission.

Freshly ground WT (Gransden) tissues were inoculated in Petri dishes of $PpNO_3$ medium, overlaid with a cellophane sheet. *Protonema* tissues were harvested after six days, 10 days or 15 days of growth in long days conditions (see above). To obtain older gametophores and spores, WT were regenerated from spores for approximately two weeks and then transferred to Magenta pots containing $PpNO_3$ medium (nine plants per pot) and cultivated in the same conditions as above. Gametophores were harvested after 35 days and then from different plants after 70 days. After 70 days, rhizoids were also harvested after first being dissected away from gametophore shoots. Both *protonema* and gametophore samples were immediately flash frozen in liquid nitrogen and kept at -80°C until RNA extraction. At 35 days the remaining pots were transferred to short day conditions (15°C, 100% hygrometry, quantum irradiance of 15 µmol m^{-2} s^{-1}) for approximately two months until capsule maturity. Capsules were sterilized (90% chlore and 10% pure ethanol) then rinsed with sterile water. Each of the four biological replicates consisted of 10-20 capsules from which spores were freed by mechanical disruption and separated from capsule debris by filtering through a 25µm nylon mesh. Spores were kept in sterile water, flash frozen in liquid nitrogen and stored at -80°C until RNA extraction. For all samples except spores, tissues were ground in liquid nitrogen using a mortar and pestle and RNA were extracted and subsequently treated with DNAse I using the Plant RNeasy Mini extraction kit (Qiagen) following the manufacturer's instructions. Spores were recovered in 1mL TRIzol reagent (Invitrogen) and crushed manually using fine pestles. RNA was separated from cell debris and protein using chloroform and then precipitated with isopropanol and washed with 70% ethanol. The spore RNA pellets were dissolved in RLT buffer from the Qiagen Plant RNeasy Mini kit and treated with DNAse I on columns following the manufacturer's instructions. 500 ng of each RNA sample was used for retro-transcription using the RevertAid H Minus Reverse Transcriptase from Thermo Fisher. Quality of obtained cDNA extracts was verified by semi-quantitative RT-PCR using the reference gene *PpAPT*. Quantitative RT-PCR reactions were carried out in 5µL using the SsoAdvanced Universal SYBR Green Supermix from BioRad and the following program on QuantStudio™ 5 (Thermo Fisher Scientific): initial denaturation at 95°C for 3 minutes, then 45 cycles of 95°C for 10 seconds and 60°C for 30 seconds. Using the CTi (for the genes of interest) and CTref (mean for the two reference genes) values obtained, relative expression (RE) was expressed as $RE = 2^{-CTi}/2^{-CTref}$.

Constructs and generation of transgenic lines

bioRxiv preprint doi: https://doi.org/10.1101/2020.11.24.395954; this version posted November 24, 2020. The copyright holder for this preprint (which was not certified by peer review) is the author/funder. All rights reserved. No reuse allowed without permission.

The expression vectors for transgenic *Arabidopsis* were constructed using the MultiSite Gateway Three-Fragment Vector Construction kit (Invitrogen). All the PpKAI2L constructs were tagged with a 6xHA epitope tag at their C-terminus. Lines were resistant to hygromycin. The AtD14 native promoter (0.8 kb) and AtKAI2 native promoter (0.7 kb) were amplified by PCR from Col-0 genomic DNA and cloned into *pDONR-P4P1R*, using Gateway recombination (Invitrogen) (see Supplementary Table 2 for primers). AtD14 CDS and AtKAI2 CDS were PCR amplified from Col-0 cDNA, PpKAI2cds were PCR amplified from *P. patens* cDNA and recombined into *pDONR221* (Invitrogen). *6xHA* with a linker (gift from U. Pedmale) was cloned into *pDONR-P2RP3* (Invitrogen). The suitable combination of promoters, CDS and 6xHA were cloned into the *pH7m34GW* final destination vectors using the three fragment recombination system (Karimi et al. 2007), and named pD14:CDS-6xHA or pKAI2:CDS-6xHA. The *Arabidopsis* At*d14-1 kai2-2* double mutant in the Landsberg background (gift from M. Waters) was transformed following the conventional dipping method (Clough and Bent 1998), with Agrobacterium strain GV3101. For all constructs, more than 12 independent T1 lines were isolated and between 2-4 representative single-insertion lines were selected in T2. Only 2-3 lines per construct were shown in these analyses. The phenotypic analysis shown in Figure 7 and Supplementary Figure 10 was performed on segregating T3 homozygous lines.

Arabidopsis hypocotyl elongation assays

Arabidopsis seeds were surface sterilized by consecutive treatments of 5 min in 70% (v/v) ethanol and 0.05% (w/v) sodium dodecyl sulfate (SDS) and 5 min in 95% (v/v) ethanol. Then seeds were sown on 0.25 X Murashige and Skoog (MS) media (Duchefa Biochemie) containing 1% agar, supplemented with 1 μM (+)-GR24, (–)-GR24 or with 0.01 % DMSO (control). Seeds were stratified at 4 °C (2 days in dark) then exposed to white light for 3 h, transferred to darkness for 21 h, and exposed to low light for 4 days at 21˚C. Plates were photographed and hypocotyl lengths were quantified using ImageJ (http://imagej.nih.gov/ij/).

Arabidopsis branching quantification

bioRxiv preprint doi: https://doi.org/10.1101/2020.11.24.395954; this version posted November 24, 2020. The copyright holder for this preprint (which was not certified by peer review) is the author/funder. All rights reserved. No reuse allowed without permission.

Experiments were carried out in summer in a greenhouse under long photoperiods (15–16 h per day); daily temperatures fluctuated between 18°C and 25°C. Peak PAR levels were between 700 and 1000 µmol m^{-2} s^{-1}. Plants were watered twice a week with tap water. The number of rosette branches longer than 5 mm was counted when the plants were 40-days-old.

Protein expression and purification

AtD14, RMS3 and AtKAI2, with cleavable GST tags were expressed and purified as described in (de Saint Germain et al. 2016). For PpKAI2L protein expression, the full length coding sequences from *P. patens* were amplified by PCR using cDNA template and specific primers (see Supplementary Table 1) containing a protease cleavage site for tag removal, and subsequently cloned into the pGEXT-4T-3 expression vector. For PpKAI2L-L, the N-terminal 47 amino acids were removed. The expression and purification of PpKAI2 proteins followed the same method as for AtD14 and AtKAI2.

Site-directed mutagenesis

Site-directed mutagenesis of *PpKAI2L-H* was performed using the QuickChange II XL Site Directed Mutagenesis kit (Stratagene), performed on pGEX-4T-3-PpKAI2L-H (see Supplementary Table 1 for primers). Mutagenesis was verified by DNA sequencing.

Enzymatic degradation of GR24 isomers by purified proteins

The ligand (10 µM) was incubated with and without purified RMS3/AtKAI2/PpKAI2L proteins (5 µM) for 150 min at 25 ºC in PBS (0.1 mL, pH = 6.8) in the presence of (±)-1-indanol (100 µM) as internal standard. The solutions were acidified to pH = 1 by addition of trifluoroacetic acid (2 µL) to quench the reaction and centrifuged (12 min, 12,000 tr/min). The samples were then subjected to RP-UPLC-MS analyses. The instrument used for all the analyses was an Ultra Performance Liquid Chromatography system equipped with a PDA and Triple Quadrupole mass spectrometer Detector (Acquity UPLC-TQD, Waters, USA). RP-UPLC (HSS C_{18} column, 1.8 µm, 2.1 mm × 50 mm) was carried out with 0.1% formic acid in CH_3CN and 0.1% formic acid in water (aq. FA, 0.1%, v/v, pH 2.8) as eluents [10% CH_3CN,

bioRxiv preprint doi: https://doi.org/10.1101/2020.11.24.395954; this version posted November 24, 2020. The copyright holder for this preprint (which was not certified by peer review) is the author/funder. All rights reserved. No reuse allowed without permission.

followed by linear gradient from 10 to 100% of CH_3CN (4 min)] at a flow rate of 0.6 mL/min. The detection was performed by PDA and using the TQD mass spectrometer operated in Electrospray ionization positive mode at 3.2 kV capillary voltage. The cone voltage and collision energy were optimized to maximize the signal and was 20 V for cone voltage and 12 eV for collision energy. The collision gas was argon at a pressure maintained near of $4.5.10^{-3}$ mBar.

Enzyme assays

Enzyme assays with pro-fluorescent probes and *p*-nitrophenyl acetate were performed as described in (de Saint Germain et al. 2016), using a TriStar LB 941 Multimode Microplate Reader from *Berthold Technologies*.

Protein melting temperature assays

Differential Scanning Fluorimetry (DSF) experiments were performed on a CFX96 Touch™ Real-Time PCR Detection System (Bio-Rad Laboratories, Inc., Hercules, California, USA) as described in (de Saint Germain et al. 2016).

nanoDSF*:* Proteins were diluted in Phosphate buffer saline (PBS) (100 mM Phosphate, pH 6.8, 150 mM NaCl) to ~10µM concentration. Ligand was tested at the concentration of 200 µM. The intrinsic fluorescence signal was measured as a function of increasing temperature in a Prometheus NT.48 fluorimeter (Nanotemper™), with 55% excitation light intensity and 1 °C/minute temperature ramp. Analyses were performed on capillaries filled with 10 µL of respective samples. The intrinsic fluorescence signal was expressed as the 350 nm/330 nm emission ratio, which increases as the proteins unfold, and was plotted as a function of temperature. The plots show one of the three independent data collections that were performed for each protein.

Intrinsic tryptophan fluorescence assays

Intrinsic tryptophan fluorescence assays and determination of the dissociation constant K_D were performed as described in (de Saint Germain et al. 2016), using a Spark® Multimode Microplate Reader from Tecan.

bioRxiv preprint doi: https://doi.org/10.1101/2020.11.24.395954; this version posted November 24, 2020. The copyright holder for this preprint (which was not certified by peer review) is the author/funder. All rights reserved. No reuse allowed without permission.

Direct ESI-MS in denaturant conditions

Mass spectrometry measurements were performed with an electrospray Q-TOF mass spectrometer (Waters) equipped with the Nanomate device (Advion, Inc.). The HD_A_384 chip (5 µm I.D. nozzle chip, flow rate range 100−500 nL/min) was calibrated before use. For ESI−MS measurements, the Q-TOF instrument was operated in RF quadrupole mode with the TOF data being collected between m/z 400−2990. Collision energy was set to 10 eV and argon was used as the collision gas. Mass spectra acquisition was performed after denaturation of PrKAI2 ± ligand in 50% acetonitrile and 1% formic acid. Mass Lynx version 4.1 (Waters) and Peakview version 2.2 (Sciex) software were used for acquisition and data processing, respectively. Deconvolution of multiply charged ions was performed by applying the MaxEnt algorithm (Sciex). The average protein masses were annotated in the spectra and the estimated mass accuracy was ± 2 Da. External calibration was performed with NaI clusters (2 µg/µL, isopropanol/H_2O 50/50, Waters) in the acquisition m/z mass range.

Localization of the ligand fixation site on PpKAI2L

PpKAI2L-ligand mixtures were incubated for 10 min before being submitted to overnight Glu-C proteolysis. Glu-C-generated peptide mixtures were analysed by nanoLC-MS/MS with the Triple-TOF 4600 mass spectrometer (AB Sciex) coupled to the nanoRSLC ultra performance liquid chromatography (UPLC) system (Thermo Scientific) equipped with a trap column (Acclaim PepMap 100 C_{18}, 75 µm i.d. × 2 cm, 3 µm) and an analytical column (Acclaim PepMap RSLC C_{18}, 75 µm i.d.× 25 cm, 2 µm, 100 Å). Peptides were loaded at 5 µL/min with 0.05% TFA in 5% acetonitrile and peptides were separated at a flow rate of 300 $nl.min^{-1}$ with a 5 to 35% solvent B gradient for 40 min. Solvent A was 0.1% formic acid in water, and solvent B was 0.1% formic acid in 100% acetonitrile. NanoLC-MS/MS experiments were conducted in Data Dependent acquisition mode by selecting the 20 most intense precursors for CID fragmentation with the Q1 quadrupole set at low resolution for better sensitivity. Raw data were processed with MS Data Converter tool (AB Sciex) for generating .mgf data files and protein identification was performed using the MASCOT search engine (Matrix Science, London, UK) against the PrKAI2 sequence with oxidation of methionines and ligand-histidine adduct as variable modifications. Peptide and fragment tolerance were respectively set at 20 ppm and 0.05 Da. Only peptides with a mascot ions score above identity threshold (25) calculated at 1% FDR were considered.

bioRxiv preprint doi: https://doi.org/10.1101/2020.11.24.395954; this version posted November 24, 2020. The copyright holder for this preprint (which was not certified by peer review) is the author/funder. All rights reserved. No reuse allowed without permission.

Homology modeling

Figures showing superimposition models were prepared using PyMOL (DeLano Scientific) with the crystal structure of AtD14 (PDB ID 4IH4) and PpKAI2L-H (PDB ID 6AZD).

Phylogenetic analysis

Phylogenic analysis was conducted using MEGA5 (Tamura et al. 2011). Protein sequences were aligned using CLUSTALX. The Maximum Likelihood method based on the Dayhoff matrix based model was used (Schwarz and Dayhoff 1979). Initial tree(s) for the heuristic search were obtained automatically as follows. When the number of common sites was < 100 or less than one fourth of the total number of sites, the maximum parsimony method was used; otherwise the BIONJ method with MCL distance matrix was used.

Statistical analyses

Kruskal-Wallis, Mann-Whitney and *post-hoc* Dunn multiple comparisons tests (details in Figures legends) were carried out either in R version 3.6.3 or in GraphPad Prism version 8.4.2. , except for Figures 11 and Supplemental Figure 14, see the legends. Unless otherwise defined, the statistical significance scores used were as follow: # $0.05 \leq p < 0.1$, * $0.01 \leq p < 0.05$, ** $0.001 \leq p < 0.01$, *** $p < 0.001$. Same letters scores indicate that $p \geq 0.05$ (non-significant differences).

ACKNOWLEDGEMENTS

The authors thank Adrian Scaffidi (University of Western Australia, Perth, Australia) for the gift of carlactone, and Mark Waters (University of Western Australia, Perth, Australia) for Arabidopsis *kai2-2* and *d14-1 kai2-2* mutants. We are grateful to Jean-Paul Pillot (IJPB) for precious help with Arabidopsis branching assays, and to Fabien Nogué (IJPB) for stimulating discussions.

AUTHOR CONTRIBUTIONS

bioRxiv preprint doi: https://doi.org/10.1101/2020.11.24.395954; this version posted November 24, 2020. The copyright holder for this preprint (which was not certified by peer review) is the author/funder. All rights reserved. No reuse allowed without permission.

SB, AdSG, ML-O and CR designed the project. ML-O, AG, F-DB, DC, BH, PLB, JBP, AdSG and SB conducted experiments. AG, ML-O, F-DB, DC, PLB, J-BP, PD, CR, AdSG and SB analyzed the data. AG and SB wrote the manuscript, with essential contributions from ML-O, F-DB, PD, CR and AdSG.

FUNDING

This research was supported by the Agence Nationale de la Recherche (contract ANR-12-BSV6-004-01). The IJPB benefits from the support of the Labex Saclay Plant Sciences-SPS (ANR-10-LABX-0040-SPS). This work was also supported by a "Infrastructures en Biologie Santé et Agronomie" grant to SICAPS platform of the Institute for Integrative Biology of the Cell, and CHARM3AT Labex program (ANR-11-LABX-39) for ICSN. A.d.S.G. is the recipient of an AgreenSkills award from the European Union in the framework of the Marie-Curie FP7 COFUND People Programme and fellowship from Saclay Plant Sciences (ANR-17-EUR-0007).

REFERENCES

Akiyama K, Matsuzaki K, Hayashi H (2005) Plant sesquiterpenes induce hyphal branching in arbuscular mycorrhizal fungi. Nature 435 (7043):824-827. doi:10.1038/nature03608

Akiyama K, Ogasawara S, Ito S, Hayashi H (2010) Structural requirements of strigolactones for hyphal branching in AM fungi. Plant Cell Physiol 51 (7):1104-1117. doi:10.1093/pcp/pcq058

Al-Babili S, Bouwmeester HJ (2015) Strigolactones, a novel carotenoid-derived plant hormone. Annu Rev Plant Biol 66:161-186. doi:10.1146/annurev-arplant-043014-114759

Alder A, Jamil M, Marzorati M, Bruno M, Vermathen M, Bigler P, Ghisla S, Bouwmeester H, Beyer P, Al-Babili S (2012) The path from beta-carotene to carlactone, a strigolactone-like plant hormone. Science 335 (6074):1348-1351. doi:10.1126/science.1218094

Besserer A, Puech-Pages V, Kiefer P, Gomez-Roldan V, Jauneau A, Roy S, Portais JC, Roux C, Becard G, Sejalon-Delmas N (2006) Strigolactones stimulate arbuscular mycorrhizal fungi by activating mitochondria. PLoS Biol 4 (7):e226

Blázquez MA, Nelson DC, Weijers D (2020) Evolution of Plant Hormone Response Pathways. Annu Rev Plant Biol 71:327-353. doi:10.1146/annurev-arplant-050718-100309

Boutet-Mercey S, Perreau F, Roux A, Clave G, Pillot JP, Schmitz-Afonso I, Touboul D, Mouille G, Rameau C, Boyer FD (2018) Validated Method for Strigolactone Quantification by Ultra High-Performance Liquid Chromatography - Electrospray Ionisation Tandem Mass Spectrometry Using Novel Deuterium Labelled Standards. Phytochem Anal 29 (1):59-68. doi:10.1002/pca.2714

bioRxiv preprint doi: https://doi.org/10.1101/2020.11.24.395954; this version posted November 24, 2020. The copyright holder for this preprint (which was not certified by peer review) is the author/funder. All rights reserved. No reuse allowed without permission.

Bowman JL, Briginshaw LN, Florent SN (2019) Evolution and co-option of developmental regulatory networks in early land plants. Curr Top Dev Biol 131:35-53. doi:10.1016/bs.ctdb.2018.10.001

Boyer FD, de Saint Germain A, Pillot JP, Pouvreau JB, Chen VX, Ramos S, Stevenin A, Simier P, Delavault P, Beau JM, Rameau C (2012) Structure-activity relationship studies of strigolactone-related molecules for branching inhibition in garden pea: molecule design for shoot branching. Plant Physiol 159 (4):1524-1544. doi:10.1104/pp.112.195826

Bürger M, Chory J (2020) The Many Models of Strigolactone Signaling. Trends Plant Sci 25 (4):395-405. doi:10.1016/j.tplants.2019.12.009

Bürger M, Mashiguchi K, Lee HJ, Nakano M, Takemoto K, Seto Y, Yamaguchi S, Chory J (2019) Structural Basis of Karrikin and Non-natural Strigolactone Perception in Physcomitrella patens. Cell Rep 26 (4):855-865.e855. doi:10.1016/j.celrep.2019.01.003

Bythell-Douglas R, Rothfels CJ, Stevenson DWD, Graham SW, Wong GK, Nelson DC, Bennett T (2017) Evolution of strigolactone receptors by gradual neo-functionalization of KAI2 paralogues. BMC biology 15 (1):52. doi:10.1186/s12915-017-0397-z

Clough SJ, Bent AF (1998) Floral dip: a simplified method for Agrobacterium-mediated transformation of Arabidopsis thaliana. Plant J 16 (6):735-743. doi:10.1046/j.1365-313x.1998.00343.x

Collonnier C, Guyon-Debast A, Maclot F, Mara K, Charlot F, Nogué F (2017) Towards mastering CRISPR-induced gene knock-in in plants: Survey of key features and focus on the model Physcomitrella patens. Methods 121-122:103-117. doi:10.1016/j.ymeth.2017.04.024

Conn CE, Bythell-Douglas R, Neumann D, Yoshida S, Whittington B, Westwood JH, Shirasu K, Bond CS, Dyer KA, Nelson DC (2015) PLANT EVOLUTION. Convergent evolution of strigolactone perception enabled host detection in parasitic plants. Science 349 (6247):540-543. doi:10.1126/science.aab1140

Conn CE, Nelson DC (2015) Evidence that KARRIKIN-INSENSITIVE2 (KAI2) Receptors may Perceive an Unknown Signal that is not Karrikin or Strigolactone. Front Plant Sci 6:1219. doi:10.3389/fpls.2015.01219

Cook CE, Whichard LP, Turner B, Wall ME, Egley GH (1966) Germination of Witchweed (Striga lutea Lour.): Isolation and Properties of a Potent Stimulant. Science 154 (3753):1189-1190

Coudert Y, Palubicki W, Ljung K, Novak O, Leyser O, Harrison CJ (2015) Three ancient hormonal cues co-ordinate shoot branching in a moss. Elife 4. doi:10.7554/eLife.06808

de Saint Germain A, Clave G, Badet-Denisot MA, Pillot JP, Cornu D, Le Caer JP, Burger M, Pelissier F, Retailleau P, Turnbull C, Bonhomme S, Chory J, Rameau C, Boyer FD (2016) An histidine covalent receptor and butenolide complex mediates strigolactone perception. Nat Chem Biol 12 (10):787-794. doi:10.1038/nchembio.2147

de Saint Germain A, Jacobs A, Brun G, Pouvreau J-B, Braem L, Cornu D, Clavé G, Baudu E, Steinmetz V, Servajean V, Wicke S, Gevaert K, Simier P, Goormachtig S, Delavault P, Boyer F-D (2020) A Phelipanche ramosa KAI2 Protein Perceives enzymatically Strigolactones and Isothiocyanates. bioRxiv:2020.2006.2009.136473. doi:10.1101/2020.06.09.136473

de Saint Germain A, Retailleau P, Norsikian S, Servajean V, Pelissier F, Steinmetz V, Pillot JP, Rochange S, Pouvreau JB, Boyer FD (2019) Contalactone, a contaminant formed

bioRxiv preprint doi: https://doi.org/10.1101/2020.11.24.395954; this version posted November 24, 2020. The copyright holder for this preprint (which was not certified by peer review) is the author/funder. All rights reserved. No reuse allowed without permission.

during chemical synthesis of the strigolactone reference GR24 is also a strigolactone mimic. Phytochemistry 168:112112. doi:10.1016/j.phytochem.2019.112112

Decker EL, Alder A, Hunn S, Ferguson J, Lehtonen MT, Scheler B, Kerres KL, Wiedemann G, Safavi-Rizi V, Nordzieke S, Balakrishna A, Baz L, Avalos J, Valkonen JPT, Reski R (2017) Strigolactone biosynthesis is evolutionarily conserved, regulated by phosphate starvation and contributes to resistance against phytopathogenic fungi in a moss, Physcomitrella patens. New Phytologist 216 (2):455-468. doi:10.1111/nph.14506

Delaux PM, Xie X, Timme RE, Puech-Pages V, Dunand C, Lecompte E, Delwiche CF, Yoneyama K, Becard G, Sejalon-Delmas N (2012) Origin of strigolactones in the green lineage. New Phytol 195 (4):857-871. doi:10.1111/j.1469-8137.2012.04209.x

Delavault P, Montiel, G., Brun, G., Pouvreau, J. B., Thoiron, S. & Simier, P. (2017) Communication Between Host Plants and Parasitic Plants. . Adv Bot Res 82:55-82. doi:0.1016/bs.abr.2016.10.006

Floková K, Shimels M, Andreo Jimenez B, Bardaro N, Strnad M, Novák O, Bouwmeester HJ (2020) An improved strategy to analyse strigolactones in complex sample matrices using UHPLC-MS/MS. Plant Methods 16:125. doi:10.1186/s13007-020-00669-3

Gomez-Roldan V, Fermas S, Brewer PB, Puech-Pages V, Dun EA, Pillot JP, Letisse F, Matusova R, Danoun S, Portais JC, Bouwmeester H, Becard G, Beveridge CA, Rameau C, Rochange SF (2008) Strigolactone inhibition of shoot branching. Nature 455 (7210):189-194. doi:10.1038/nature07271

Guillory A, Bonhomme S (2021) Methods for medium-scale study of Strigolactone-like molecules' biological effects on the moss Physcomitrella patens In: SpringerNature (ed) Strigolactones.

Gutjahr C, Gobbato E, Choi J, Riemann M, Johnston MG, Summers W, Carbonnel S, Mansfield C, Yang SY, Nadal M, Acosta I, Takano M, Jiao WB, Schneeberger K, Kelly KA, Paszkowski U (2015) Rice perception of symbiotic arbuscular mycorrhizal fungi requires the karrikin receptor complex. Science 350 (6267):1521-1524. doi:10.1126/science.aac9715

Harris BJ, Harrison CJ, Hetherington AM, Williams TA (2020) Phylogenomic Evidence for the Monophyly of Bryophytes and the Reductive Evolution of Stomata. Curr Biol 30 (11):2001-2012.e2002. doi:10.1016/j.cub.2020.03.048

Hoffmann B, Proust H, Belcram K, Labrune C, Boyer FD, Rameau C, Bonhomme S (2014) Strigolactones inhibit caulonema elongation and cell division in the moss Physcomitrella patens. PLoS One 9 (6):e99206. doi:10.1371/journal.pone.0099206

Huet S, Pouvreau J-B, Delage E, Delgrange S, Marais C, Bahut M, Delavault P, Simier P, Poulin L (2020) Populations of the Parasitic Plant Phelipanche ramosa Influence Their Seed Microbiota. Front Plant Sci 11 (1075). doi:10.3389/fpls.2020.01075

Jamil M, Kountche BA, Wang JY, Haider I, Jia KP, Takahashi I, Ota T, Asami T, Al-Babili S (2020) A New Series of Carlactonoic Acid Based Strigolactone Analogs for Fundamental and Applied Research. Front Plant Sci 11:434. doi:10.3389/fpls.2020.00434

Karimi M, Bleys A, Vanderhaeghen R, Hilson P (2007) Building blocks for plant gene assembly. Plant Physiol 145 (4):1183-1191. doi:10.1104/pp.107.110411

Lang D, Zimmer AD, Rensing SA, Reski R (2008) Exploring plant biodiversity: the Physcomitrella genome and beyond. Trends Plant Sci 13 (10):542-549. doi:10.1016/j.tplants.2008.07.002

Li W, Nguyen KH, Chu HD, Watanabe Y, Osakabe Y, Sato M, Toyooka K, Seo M, Tian L, Tian C, Yamaguchi S, Tanaka M, Seki M, Tran LP (2020) Comparative functional

bioRxiv preprint doi: https://doi.org/10.1101/2020.11.24.395954; this version posted November 24, 2020. The copyright holder for this preprint (which was not certified by peer review) is the author/funder. All rights reserved. No reuse allowed without permission.

analyses of DWARF14 and KARRIKIN INSENSITIVE 2 in drought adaptation of Arabidopsis thaliana. Plant J. doi:10.1111/tpj.14712

Lopez-Obando M, Conn CE, Hoffmann B, Bythell-Douglas R, Nelson DC, Rameau C, Bonhomme S (2016a) Structural modelling and transcriptional responses highlight a clade of PpKAI2-LIKE genes as candidate receptors for strigolactones in Physcomitrella patens. Planta 243 (6):1441-1453. doi:10.1007/s00425-016-2481-y

Lopez-Obando M, de Villiers R, Hoffmann B, Ma L, de Saint Germain A, Kossmann J, Coudert Y, Harrison CJ, Rameau C, Hills P, Bonhomme S (2018) Physcomitrella patens MAX2 characterization suggests an ancient role for this F-box protein in photomorphogenesis rather than strigolactone signalling. New Phytol 219 (2):743-756. doi:10.1111/nph.15214

Lopez-Obando M, Hoffmann B, Géry C, Guyon-Debast A, Téoulé E, Rameau C, Bonhomme S, Nogué F (2016b) Simple and Efficient Targeting of Multiple Genes Through CRISPR-Cas9 in Physcomitrella patens. G3 (Bethesda) 6 (11):3647-3653. doi:10.1534/g3.116.033266

Lopez-Obando M, Ligerot Y, Bonhomme S, Boyer F-D, Rameau C (2015) Strigolactone biosynthesis and signaling in plant development. Development 142 (21):3615-3619. doi:10.1242/dev.120006

Mizuno Y, Komatsu A, Shimazaki S, Xie X, Ishizaki K, Naramoto S, Kyozuka J (2020) Major components in the KARRIKIN INSENSITIVE2-ligand signaling pathway are conserved in the liverwort, Marchantia polymorpha. bioRxiv:2020.2011.2017.387852. doi:10.1101/2020.11.17.387852

Nelson DC, Scaffidi A, Dun EA, Waters MT, Flematti GR, Dixon KW, Beveridge CA, Ghisalberti EL, Smith SM (2011) F-box protein MAX2 has dual roles in karrikin and strigolactone signaling in Arabidopsis thaliana. Proc Natl Acad Sci U S A 108 (21):8897-8902. doi:10.1073/pnas.1100987108

Ortiz-Ramirez C, Hernandez-Coronado M, Thamm A, Catarino B, Wang M, Dolan L, Feijo JA, Becker JD (2016) A Transcriptome Atlas of Physcomitrella patens Provides Insights into the Evolution and Development of Land Plants. Mol Plant 9 (2):205-220. doi:10.1016/j.molp.2015.12.002

Pouvreau JB, Gaudin Z, Auger B, Lechat MM, Gauthier M, Delavault P, Simier P (2013) A high-throughput seed germination assay for root parasitic plants. Plant Methods 9 (1):32. doi:10.1186/1746-4811-9-32

Proust H, Hoffmann B, Xie X, Yoneyama K, Schaefer DG, Nogue F, Rameau C (2011) Strigolactones regulate protonema branching and act as a quorum sensing-like signal in the moss Physcomitrella patens. Development 138 (8):1531-1539. doi:10.1242/dev.058495

Puttick MN, Morris JL, Williams TA, Cox CJ, Edwards D, Kenrick P, Pressel S, Wellman CH, Schneider H, Pisani D, Donoghue PCJ (2018) The Interrelationships of Land Plants and the Nature of the Ancestral Embryophyte. Curr Biol 28 (5):733-745.e732. doi:10.1016/j.cub.2018.01.063

Rial C, Varela RM, Molinillo JMG, López-Ráez JA, Macías FA (2019) A new UHPLC-MS/MS method for the direct determination of strigolactones in root exudates and extracts. Phytochem Anal 30 (1):110-116. doi:10.1002/pca.2796

Scaffidi A, Waters MT, Sun YK, Skelton BW, Dixon KW, Ghisalberti EL, Flematti GR, Smith SM (2014) Strigolactone Hormones and Their Stereoisomers Signal through Two Related Receptor Proteins to Induce Different Physiological Responses in Arabidopsis. Plant Physiol 165 (3):1221-1232. doi:10.1104/pp.114.240036

bioRxiv preprint doi: https://doi.org/10.1101/2020.11.24.395954; this version posted November 24, 2020. The copyright holder for this preprint (which was not certified by peer review) is the author/funder. All rights reserved. No reuse allowed without permission.

Schwarz R, Dayhoff M (1979) Matrices for Detecting Distant Relationships. In: Dayhoff M (ed) Atlas of Protein Sequences, National Biomedical Research Foundation. National Biomedical Research Foundation, Washington, DC, pp 353-358

Seto Y, Yasui R, Kameoka H, Tamiru M, Cao M, Terauchi R, Sakurada A, Hirano R, Kisugi T, Hanada A, Umehara M, Seo E, Akiyama K, Burke J, Takeda-Kamiya N, Li W, Hirano Y, Hakoshima T, Mashiguchi K, Noel JP, Kyozuka J, Yamaguchi S (2019) Strigolactone perception and deactivation by a hydrolase receptor DWARF14. Nat Commun 10 (1):191. doi:10.1038/s41467-018-08124-7

Shabek N, Ticchiarelli F, Mao H, Hinds TR, Leyser O, Zheng N (2018) Structural plasticity of D3-D14 ubiquitin ligase in strigolactone signalling. Nature 563 (7733):652-656. doi:10.1038/s41586-018-0743-5

Soundappan I, Bennett T, Morffy N, Liang Y, Stanga JP, Abbas A, Leyser O, Nelson D (2015) SMAX1-LIKE/D53 Family Members Enable Distinct MAX2-Dependent Responses to Strigolactones and Karrikins in Arabidopsis. The Plant Cell 27 (11):3143-3159. doi:10.1105/tpc.15.00562

Stojanova B, Delourme R, Duffé P, Delavault P, Simier P (2019) Genetic differentiation and host preference reveal non-exclusive host races in the generalist parasitic weed Phelipanche ramosa. Weed Research 59 (2):107-118. doi:10.1111/wre.12353

Sun X, Chen F, Yuan L, Mi G (2020) The physiological mechanism underlying root elongation in response to nitrogen deficiency in crop plants. Planta 251 (4):84. doi:10.1007/s00425-020-03376-4

Tamura K, Peterson D, Peterson N, Stecher G, Nei M, Kumar S (2011) MEGA5: molecular evolutionary genetics analysis using maximum likelihood, evolutionary distance, and maximum parsimony methods. Mol Biol Evol 28 (10):2731-2739. doi:10.1093/molbev/msr121

Thelander M, Nilsson A, Olsson T, Johansson M, Girod PA, Schaefer DG, Zryd JP, Ronne H (2007) The moss genes PpSKI1 and PpSKI2 encode nuclear SnRK1 interacting proteins with homologues in vascular plants. Plant Mol Biol 64 (5):559-573. doi:10.1007/s11103-007-9176-5

Toh S, Holbrook-Smith D, Stogios PJ, Onopriyenko O, Lumba S, Tsuchiya Y, Savchenko A, McCourt P (2015) Structure-function analysis identifies highly sensitive strigolactone receptors in Striga. Science 350 (6257):203-207. doi:10.1126/science.aac9476

Trouiller B, Schaefer DG, Charlot F, Nogue F (2006) MSH2 is essential for the preservation of genome integrity and prevents homeologous recombination in the moss Physcomitrella patens. Nucleic Acids Res 34 (1):232-242. doi:10.1093/nar/gkj423

Umehara M, Hanada A, Yoshida S, Akiyama K, Arite T, Takeda-Kamiya N, Magome H, Kamiya Y, Shirasu K, Yoneyama K, Kyozuka J, Yamaguchi S (2008) Inhibition of shoot branching by new terpenoid plant hormones. Nature 455 (7210):195-200. doi:10.1038/nature07272

Villaecija-Aguilar JA, Hamon-Josse M, Carbonnel S, Kretschmar A, Schmidt C, Dawid C, Bennett T, Gutjahr C (2019) SMAX1/SMXL2 regulate root and root hair development downstream of KAI2-mediated signalling in Arabidopsis. PLoS genetics 15 (8):e1008327. doi:10.1371/journal.pgen.1008327

Walker CH, Siu-Ting K, Taylor A, O'Connell MJ, Bennett T (2019) Strigolactone synthesis is ancestral in land plants, but canonical strigolactone signalling is a flowering plant innovation. BMC biology 17 (1):70. doi:10.1186/s12915-019-0689-6

Wang L, Waters MT, Smith SM (2018) Karrikin-KAI2 signalling provides Arabidopsis seeds with tolerance to abiotic stress and inhibits germination under conditions unfavourable to seedling establishment. New Phytol 219 (2):605-618. doi:10.1111/nph.15192

bioRxiv preprint doi: https://doi.org/10.1101/2020.11.24.395954; this version posted November 24, 2020. The copyright holder for this preprint (which was not certified by peer review) is the author/funder. All rights reserved. No reuse allowed without permission.

Waters MT, Gutjahr C, Bennett T, Nelson DC (2017) Strigolactone Signaling and Evolution. Annu Rev Plant Biol 68:291-322. doi:10.1146/annurev-arplant-042916-040925

Waters MT, Nelson DC, Scaffidi A, Flematti GR, Sun YK, Dixon KW, Smith SM (2012) Specialisation within the DWARF14 protein family confers distinct responses to karrikins and strigolactones in Arabidopsis. Development 139 (7):1285-1295. doi:10.1242/dev.074567

Waters MT, Scaffidi A, Flematti G, Smith SM (2015a) Substrate-Induced Degradation of the alpha/beta-Fold Hydrolase KARRIKIN INSENSITIVE2 Requires a Functional Catalytic Triad but Is Independent of MAX2. Mol Plant 8 (5):814-817. doi:10.1016/j.molp.2014.12.020

Waters MT, Scaffidi A, Moulin SL, Sun YK, Flematti GR, Smith SM (2015b) A Selaginella moellendorffii Ortholog of KARRIKIN INSENSITIVE2 Functions in Arabidopsis Development but Cannot Mediate Responses to Karrikins or Strigolactones. Plant Cell 27 (7):1925-1944. doi:10.1105/tpc.15.00146

Xie X (2016) Structural diversity of strigolactones and their distribution in the plant kingdom. J Pestic Sci 41 (4):175-180. doi:10.1584/jpestics.J16-02

Yao R, Ming Z, Yan L, Li S, Wang F, Ma S, Yu C, Yang M, Chen L, Chen L, Li Y, Yan C, Miao D, Sun Z, Yan J, Sun Y, Wang L, Chu J, Fan S, He W, Deng H, Nan F, Li J, Rao Z, Lou Z, Xie D (2016) DWARF14 is a non-canonical hormone receptor for strigolactone. Nature 536 (7617):469-473. doi:10.1038/nature19073

Yoneyama K (2020) Recent progress in the chemistry and biochemistry of strigolactones. J Pestic Sci. doi:doi:10.1584/jpestics.D19-084

Yoneyama K, Mori N, Sato T, Yoda A, Xie X, Okamoto M, Iwanaga M, Ohnishi T, Nishiwaki H, Asami T, Yokota T, Akiyama K, Yoneyama K, Nomura T (2018a) Conversion of carlactone to carlactonoic acid is a conserved function of MAX1 homologs in strigolactone biosynthesis. New Phytol 218 (4):1522-1533. doi:10.1111/nph.15055

Yoneyama K, Xie X, Yoneyama K, Kisugi T, Nomura T, Nakatani Y, Akiyama K, McErlean CSP (2018b) Which are the major players, canonical or non-canonical strigolactones? J Exp Bot 69 (9):2231-2239. doi:10.1093/jxb/ery090

Zheng J, Hong K, Zeng L, Wang L, Kang S, Qu M, Dai J, Zou L, Zhu L, Tang Z, Meng X, Wang B, Hu J, Zeng D, Zhao Y, Cui P, Wang Q, Qian Q, Wang Y, Li J, Xiong G (2020) Karrikin Signaling Acts Parallel to and Additively with Strigolactone Signaling to Regulate Rice Mesocotyl Elongation in Darkness. Plant Cell 32 (9):2780-2805. doi:10.1105/tpc.20.00123

The *Physcomitrium (Physcomitrella) patens PpKAI2L* receptors for strigolactones and related compounds highlight MAX2 dependent and independent pathways

Mauricio Lopez-Obando[1], Ambre Guillory[1], François-Didier Boyer, David Cornu, Beate Hoffmann, Philippe Le Bris, Jean-Bernard Pouvreau, Philippe Delavault, Catherine Rameau, Alexandre de Saint Germain*, Sandrine Bonhomme*.

[1]co-first author

*Corresponding author

13 Figures
3 suppl tables
14 suppl figures

Figure 1

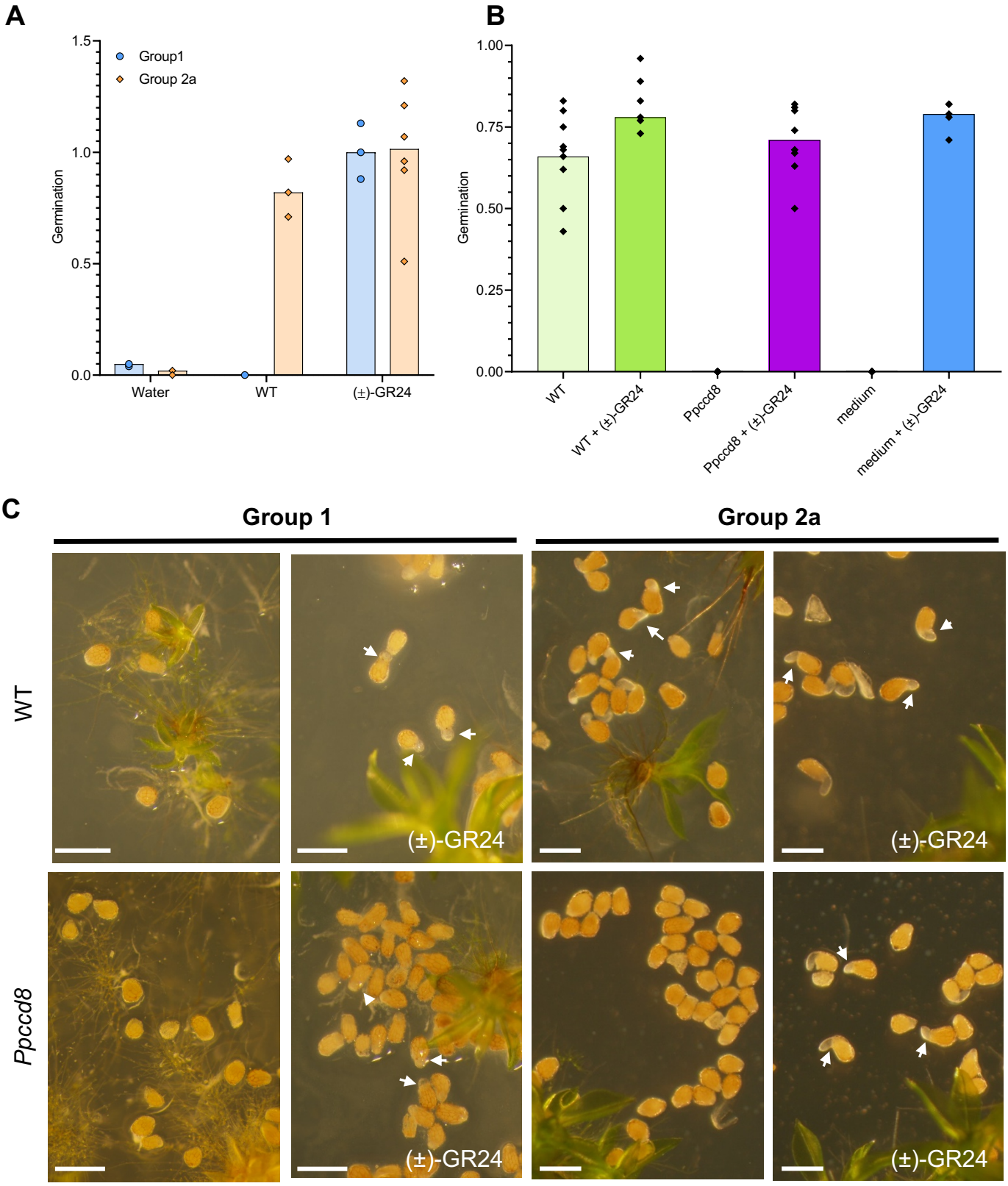
A
Group1
Group 2a
Germination
1.5
1.0
0.5
0.0
Water
WT
(±)-GR24
B
Germination
1.00
0.75
0.50
0.25
0.00
WT
WT + (±)-GR24
Ppccd8
Ppccd8 + (±)-GR24
medium
medium + (±)-GR24
C
Group 1
Group 2a
WT
Ppccd8
(±)-GR24
(±)-GR24
(±)-GR24
(±)-GR24

Figure 1: PpCCD8-derived compounds are germination stimulants (GS) of a specific group of *Phelipanche ramosa.*

(A) GS activities of *P. patens* exudates on *P. ramosa* group 1 and 2a seeds relative to 0.1 µM (±)-GR24. **(B)** Germination rate of seeds of *P. ramosa* group 2a on plates with *P. patens* WT, *Ppccd8* mutant plants, or with culture medium only, with or without 0.1 µM (±)-GR24. **(C)** Seeds from *P. ramosa* group1 (left) and group 2a (right) on plates with WT (top) or *Ppccd8* mutant plants (bottom), with or without 0.1 µM(±)-GR24. Arrows indicate germinating seeds. Scale bar = 0.5 mm.

Figure 2

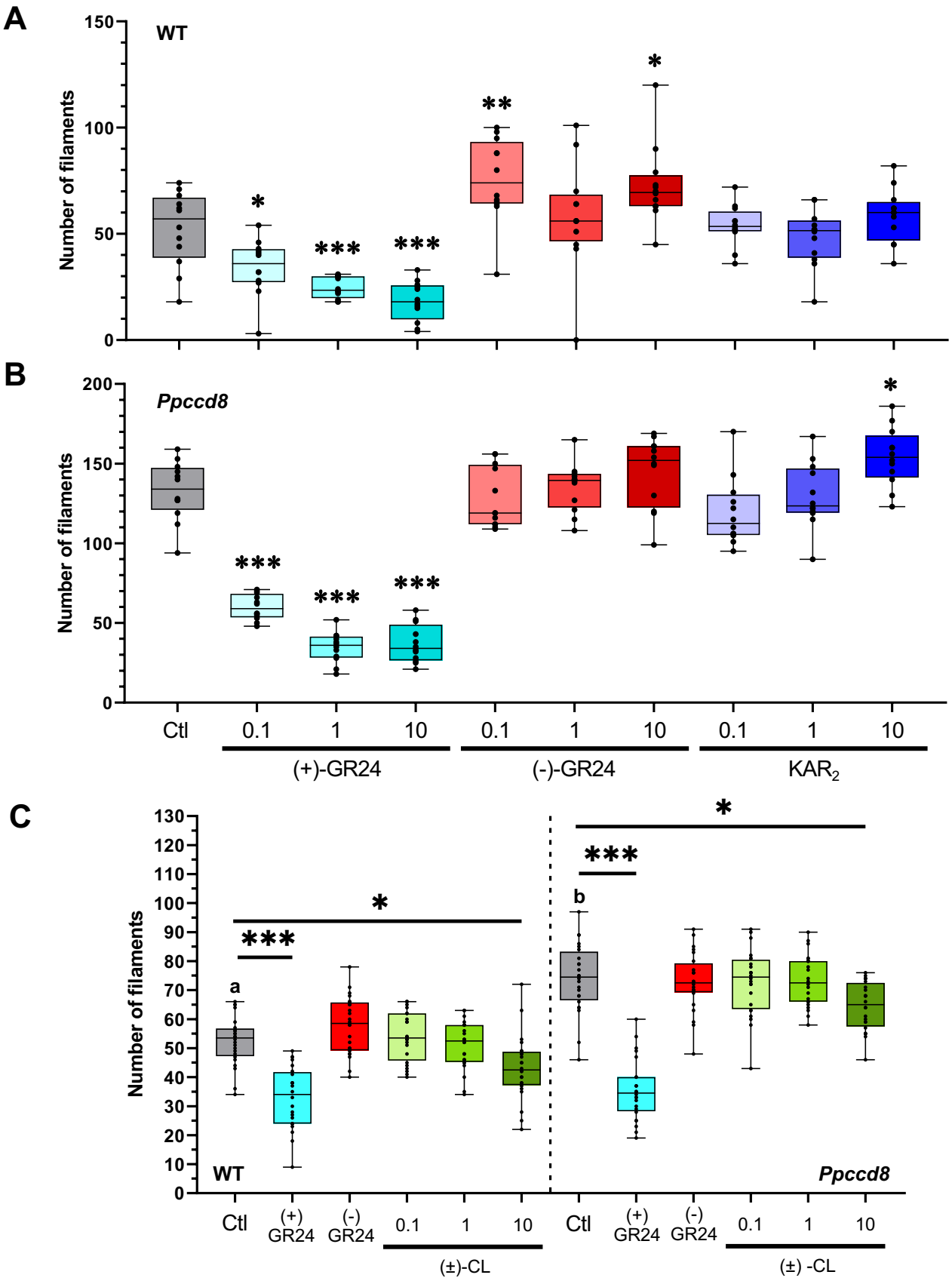
A
WT
Number of filaments
150
100
50
0
*
***
***
**
*
B
Ppccd8
Number of filaments
200
150
100
50
0
***
***
***
*
Ctl
0.1
1
10
0.1
1
10
0.1
1
10
(+)-GR24
(-)-GR24
KAR2
C
Number of filaments
130
120
110
100
90
80
70
60
50
40
30
20
10
0
*
***
a
b
*
***
WT
Ppccd8
Ctl
(+) GR24
(-) GR24
0.1
1
10
Ctl
(+) GR24
(-) GR24
0.1
1
10
(±)-CL
(±) -CL

Figure 2: Phenotypic response to (+)- and (−)-GR24 enantiomers and natural compounds: number of *caulonema* filaments. *Caulonema* filaments were counted for WT **(A)** and the *Ppccd8* SL synthesis mutant **(B)** grown for 10 days vertically in the dark, following application of increasing concentrations (0.1, 1 and 10 µM) of (+)-GR24 (blue boxes), (−)-GR24 (red boxes) and $KAR_{2,}$ (dark blue boxes). Control: 0.01% DMSO. (**C**) *Caulonema* filament numbers of WT and *Ppccd8* mutant grown for 10 days vertically in the dark, following application of increasing concentrations (0.1, 1 and 10 µM) of (±)-CL (green boxes). Control (Ctl): 0.01% DMSO. (+)-GR24 (blue boxes) and (−)-GR24 (red boxes) were applied at 1 µM. Significant differences between control and treated plants within a genotype based on a Kruskal-Wallis test, followed by a Dunn *post-hoc* test for multiple comparisons: ***, P<0.001; **, P<0.01; *, P<0.5; For each genotype and treatment, n = 24 plants grown in three different 24 well-plates.

Figure 3

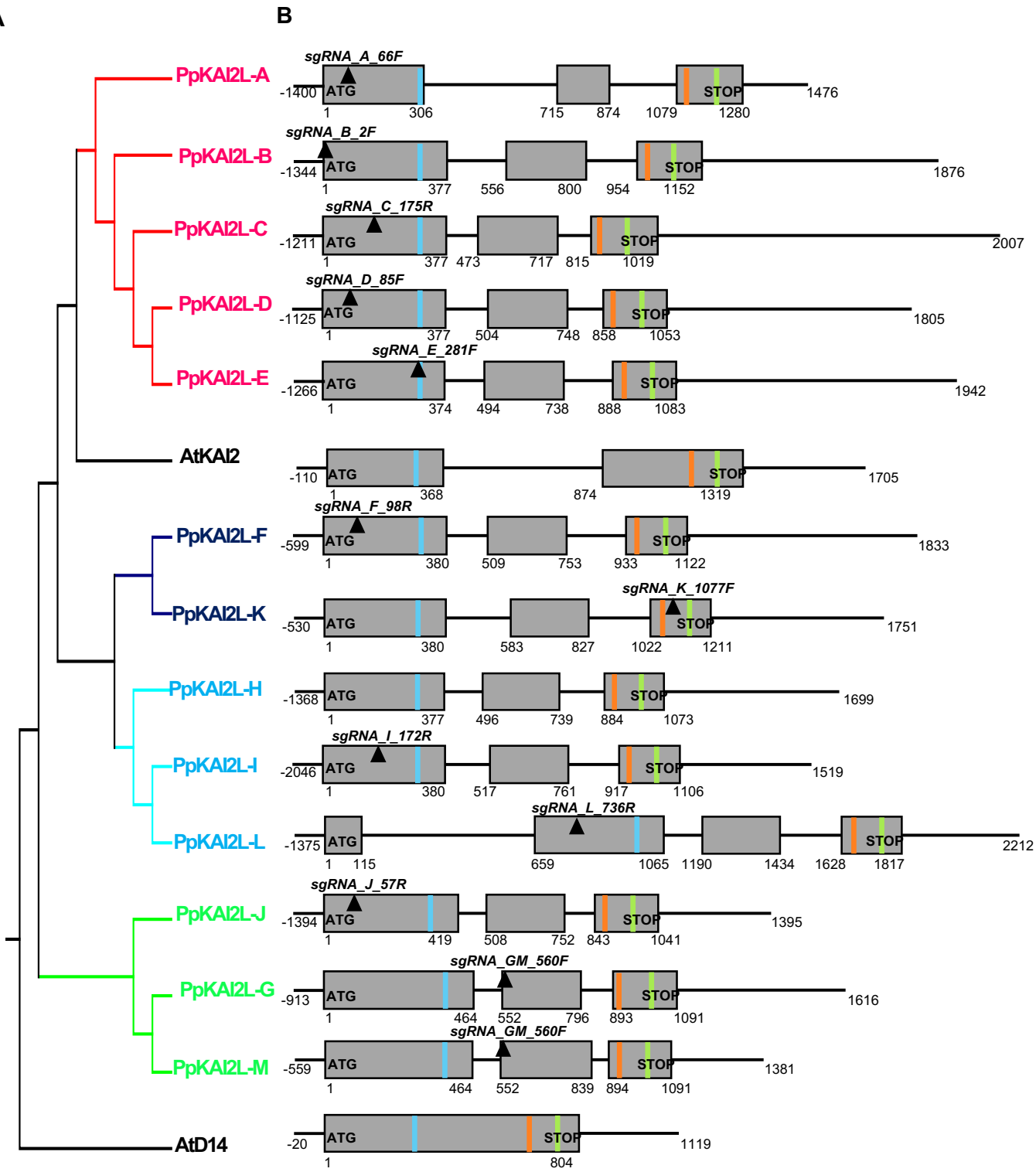
A
B
PpKAI2L-A
PpKAI2L-B
PpKAI2L-C
PpKAI2L-D
PpKAI2L-E
AtKAI2
PpKAI2L-F
PpKAI2L-K
PpKAI2L-H
PpKAI2L-I
PpKAI2L-L
PpKAI2L-J
PpKAI2L-G
PpKAI2L-M
AtD14
sgRNA_A_66F
-1400 ATG STOP 1476
1 306 715 874 1079 1280
sgRNA_B_2F
-1344 ATG STOP 1876
1 377 556 800 954 1152
sgRNA_C_175R
-1211 ATG STOP 2007
1 377 473 717 815 1019
sgRNA_D_85F
-1125 ATG STOP 1805
1 377 504 748 858 1053
sgRNA_E_281F
-1266 ATG STOP 1942
1 374 494 738 888 1083
-110 ATG STOP 1705
1 368 874 1319
sgRNA_F_98R
-599 ATG STOP 1833
1 380 509 753 933 1122
sgRNA_K_1077F
-530 ATG STOP 1751
1 380 583 827 1022 1211
-1368 ATG STOP 1699
1 377 496 739 884 1073
sgRNA_I_172R
-2046 ATG STOP 1519
1 380 517 761 917 1106
sgRNA_L_736R
-1375 ATG STOP 2212
1 115 659 1065 1190 1434 1628 1817
sgRNA_J_57R
-1394 ATG STOP 1395
1 419 508 752 843 1041
sgRNA_GM_560F
-913 ATG STOP 1616
1 464 552 796 893 1091
sgRNA_GM_560F
-559 ATG STOP 1381
1 464 552 839 894 1091
-20 ATG STOP 1119
1 804

Figure 3 Phylogeny and models of the *PpKAI2L* gene family.

(A) Phylogenic tree of PpKAI2-LIKE proteins and paralogs from *Arabidopsis thaliana* (At) using the Maximum Likelihood method based on the Dayhoff matrix-based model. The tree with the highest log likelihood is shown. Numbers are percent bootstrap values for 1000 replicates. The tree is drawn to scale, with branch lengths measured as the number of substitutions per site. Evolutionary analyses were conducted in MEGA5. **(B)** Gene diagrams. Exons are displayed as grey boxes, introns and UTRs are depicted as thin black lines. Start and Stop codons are written in bold, while plain text indicates the start/end position for each feature, relative to the start codon. Only 5'-UTR regions are not represented true to scale. Transcript versions that were used are V3.1 (downloaded from the Phytozome website in September 2019) for all *PpKAI2L* genes except for *PpKAI2L-B*, *PpKAI2L-H* and *PpKAI2L-M* (V3.2). Regions targeted by guide RNAs are indicated by black inverted triangles, with their names written in bold italic. Light blue, orange and light green bands represent respectively the codons for the S, D and H residues of the catalytic triad (see Supplemental Table 3 for reference sequences).

Figure 4

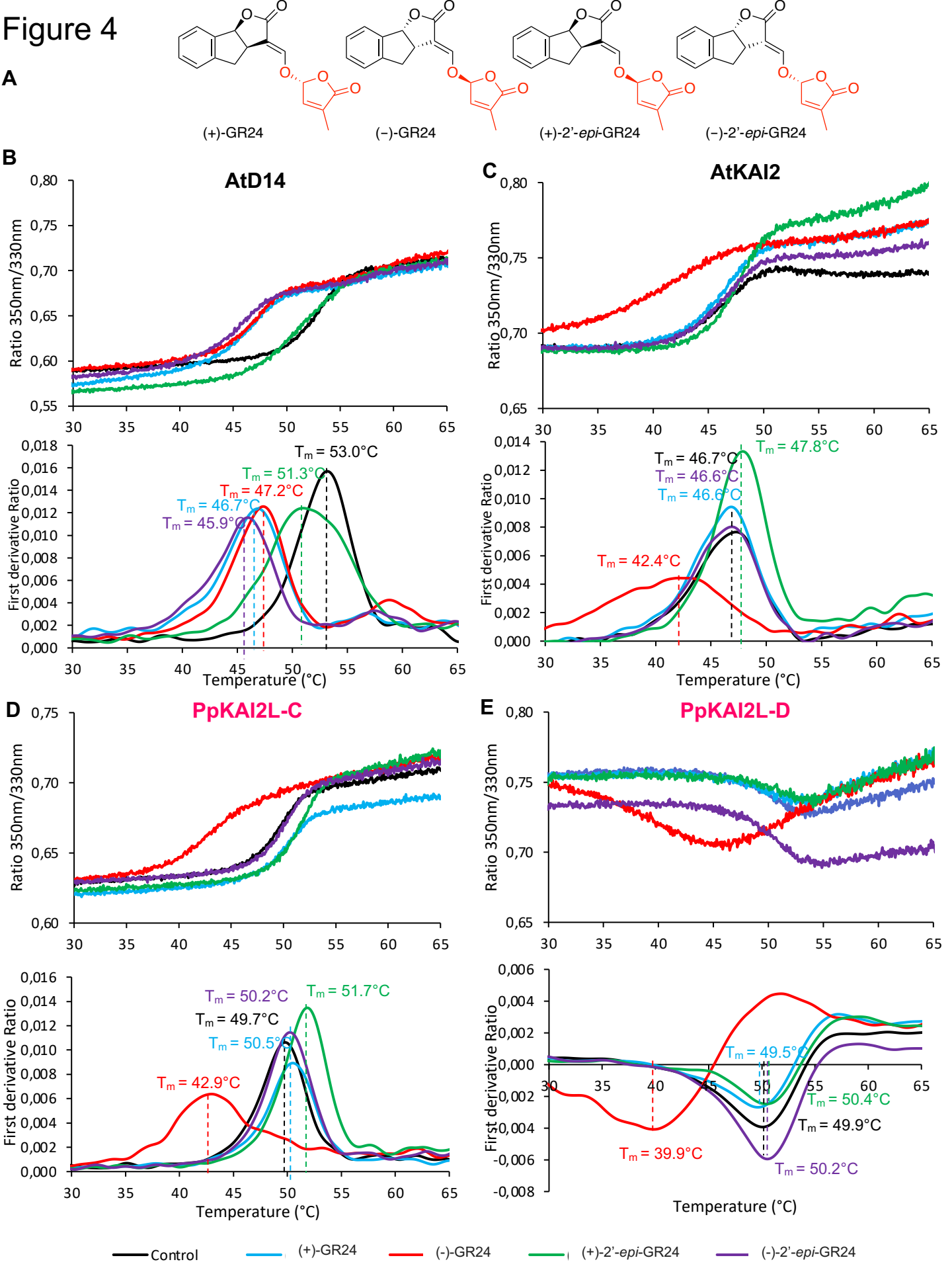
A
(+)-GR24
(−)-GR24
(+)-2'-epi-GR24
(−)-2'-epi-GR24
B
AtD14
Ratio 350nm/330nm
First derivative Ratio
Temperature (°C)
Tm = 53.0°C
Tm = 51.3°C
Tm = 47.2°C
Tm = 46.7°C
Tm = 45.9°C
C
AtKAI2
Tm = 47.8°C
Tm = 46.7°C
Tm = 46.6°C
Tm = 46.6°C
Tm = 42.4°C
D
PpKAI2L-C
Tm = 50.2°C
Tm = 51.7°C
Tm = 49.7°C
Tm = 50.5°C
Tm = 42.9°C
E
PpKAI2L-D
Tm = 49.5°C
Tm = 50.4°C
Tm = 49.9°C
Tm = 39.9°C
Tm = 50.2°C
Control
(+)-GR24
(-)-GR24
(+)-2'-epi-GR24
(-)-2'-epi-GR24

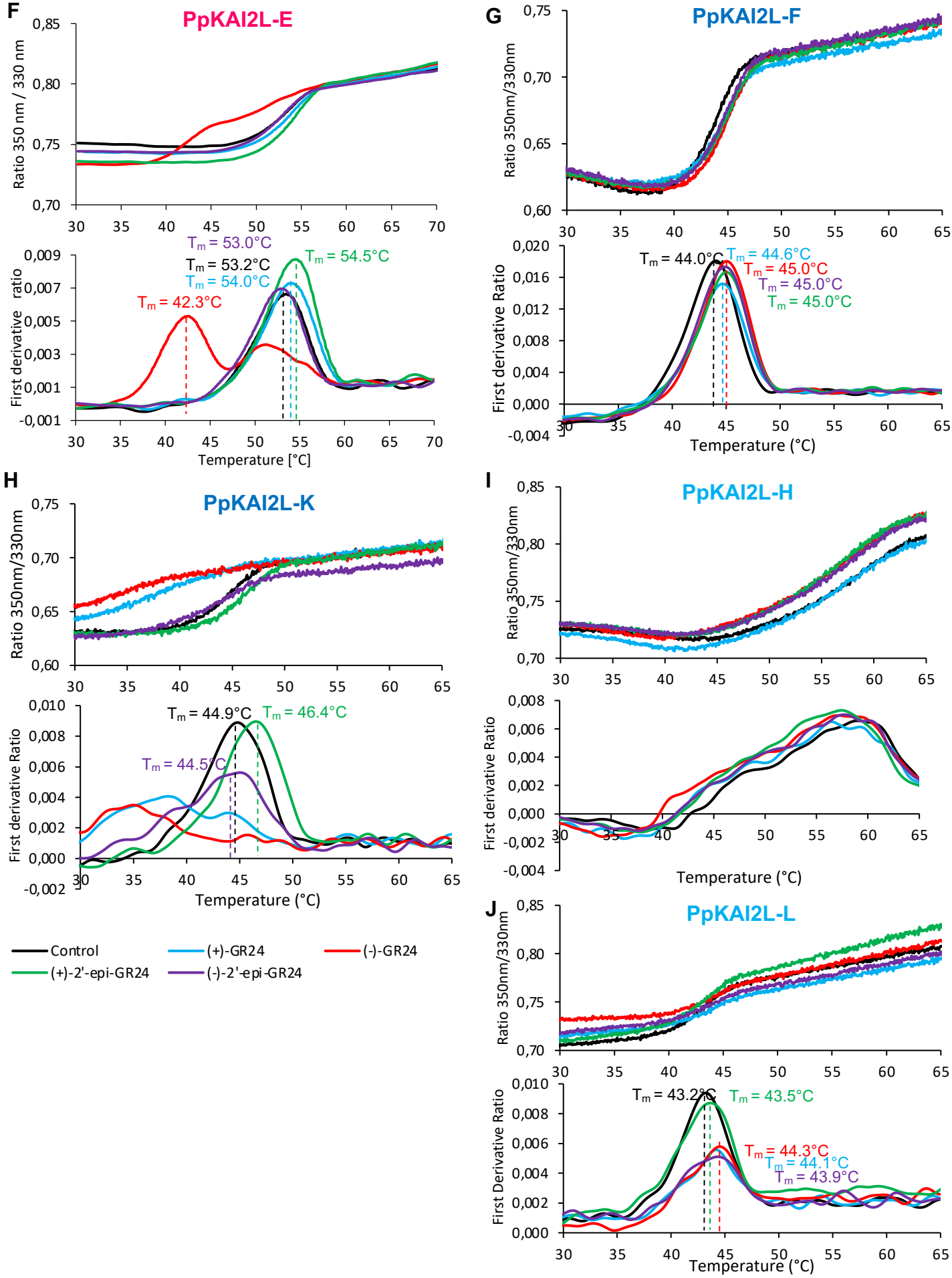
F
PpKAI2L-E
Ratio 350 nm / 330 nm
First derivative ratio
Temperature [°C]
Tm = 53.0°C
Tm = 53.2°C
Tm = 54.0°C
Tm = 54.5°C
Tm = 42.3°C
G
PpKAI2L-F
Ratio 350nm/330nm
First derivative Ratio
Temperature (°C)
Tm = 44.0°C
Tm = 44.6°C
Tm = 45.0°C
Tm = 45.0°C
Tm = 45.0°C
H
PpKAI2L-K
Ratio 350nm/330nm
First derivative Ratio
Temperature (°C)
Tm = 44.9°C
Tm = 46.4°C
Tm = 44.5°C
I
PpKAI2L-H
Ratio 350nm/330nm
First derivative Ratio
Temperature (°C)
J
PpKAI2L-L
Ratio 350nm/330nm
First Derivative Ratio
Temperature (°C)
Tm = 43.2°C
Tm = 43.5°C
Tm = 44.3°C
Tm = 44.1°C
Tm = 43.9°C
Control
(+)-GR24
(-)-GR24
(+)-2'-epi-GR24
(-)-2'-epi-GR24

Figure 4: Nano Differential Scanning Fluorimetry (nanoDSF) analysis of the PpKAI2L protein response to GR24 isomers .

(**A**) Chemical structures of GR24 isomers. (**B-J**) Thermostability of AtD14, AtKAI2 and PpKAI2 proteins at 10 µM in the absence of a ligand (black line) or in the presence of various ligands: (+)-GR24 (blue line), (–)-GR24 (red line), (+)-2'-*epi*-GR24 (green line) and (–)-2'-*epi*-GR24 (purple line) at 100 µM analyzed by nanoDSF. For each protein the top panels show the changes in fluorescence (ratio F_{350nm}/F_{330nm}) with temperature. The bottom panels show the first derivatives for the F_{350nm}/F_{330nm} curve against the temperature gradient from which the apparent melting temperatures (T_m) for each sample was determined. The experiment was carried out twice.

Figure 5

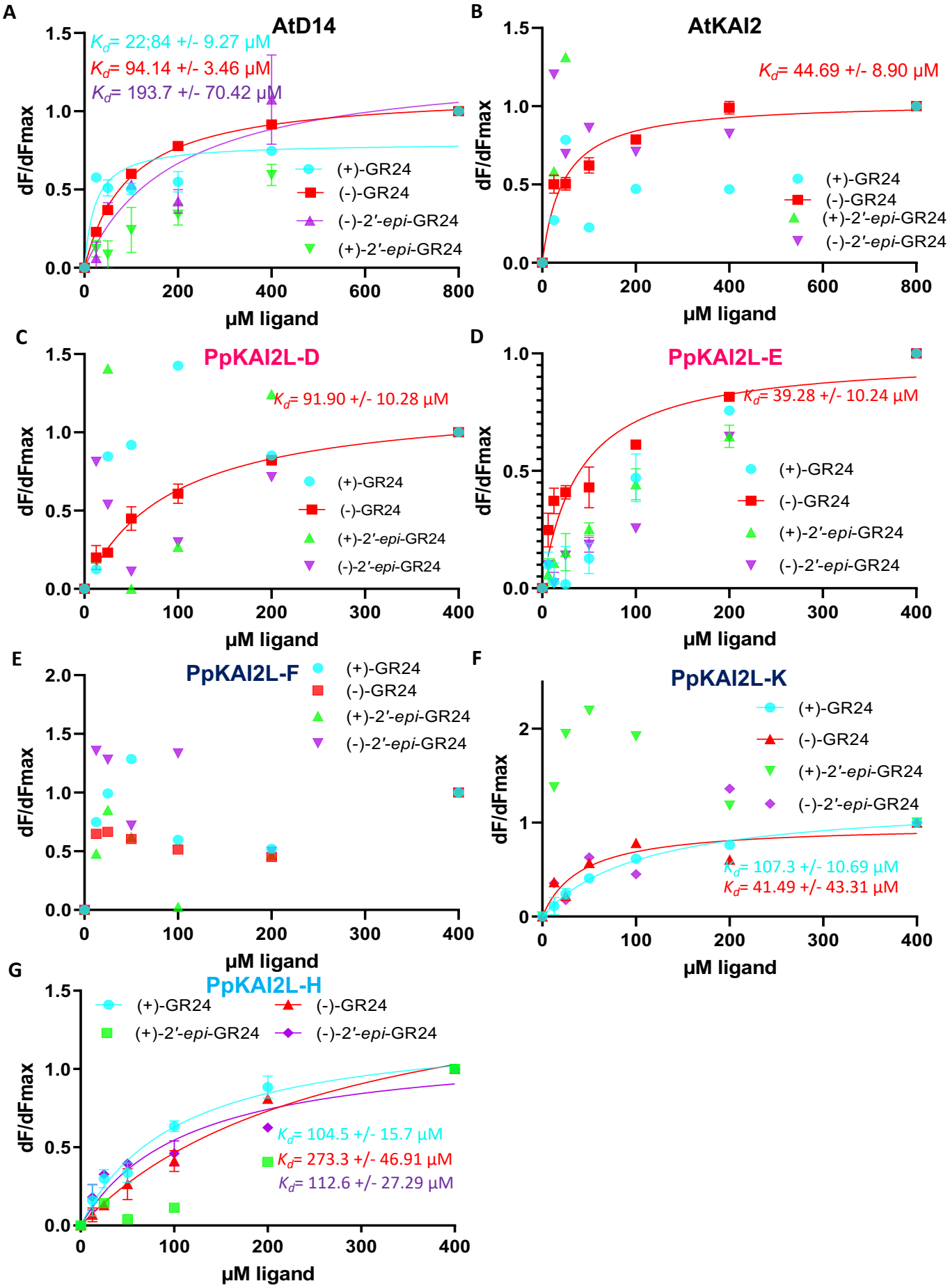
A
AtD14
K_d= 22;84 +/- 9.27 µM
K_d= 94.14 +/- 3.46 µM
K_d= 193.7 +/- 70.42 µM
(+)-GR24
(-)-GR24
(-)-2′-epi-GR24
(+)-2′-epi-GR24
dF/dFmax
µM ligand
B
AtKAI2
K_d= 44.69 +/- 8.90 µM
(+)-GR24
(-)-GR24
(+)-2′-epi-GR24
(-)-2′-epi-GR24
dF/dFmax
µM ligand
C
PpKAI2L-D
K_d= 91.90 +/- 10.28 µM
(+)-GR24
(-)-GR24
(+)-2′-epi-GR24
(-)-2′-epi-GR24
dF/dFmax
µM ligand
D
PpKAI2L-E
K_d= 39.28 +/- 10.24 µM
(+)-GR24
(-)-GR24
(+)-2′-epi-GR24
(-)-2′-epi-GR24
dF/dFmax
µM ligand
E
PpKAI2L-F
(+)-GR24
(-)-GR24
(+)-2′-epi-GR24
(-)-2′-epi-GR24
dF/dFmax
µM ligand
F
PpKAI2L-K
(+)-GR24
(-)-GR24
(+)-2′-epi-GR24
(-)-2′-epi-GR24
K_d= 107.3 +/- 10.69 µM
K_d= 41.49 +/- 43.31 µM
dF/dFmax
µM ligand
G
PpKAI2L-H
(+)-GR24
(-)-GR24
(+)-2′-epi-GR24
(-)-2′-epi-GR24
K_d= 104.5 +/- 15.7 µM
K_d= 273.3 +/- 46.91 µM
K_d= 112.6 +/- 27.29 µM
dF/dFmax
µM ligand

Figure 5: Intrinsic tryptophan fluorescence shows that GR24 isomers bind to PpKAI2L proteins with different affinities.

Plots of fluorescence intensity *versus* isomer concentrations. The change in intrinsic fluorescence of AtD14 **(A)**; AtKAI2 **(B)**; PpKAI2L-D **(C)**; PpKAI2L-E; **(D)** PpKAI2L-F **(E)**; PpKAI2L-K **(F);** and PpKAI2L-H **(G)** was monitored (see Supplementary Figure 4) and used to determine the apparent K_d values. The plots represent the mean of two replicates and the experiments were repeated at least three times. The analysis was performed with GraphPad Prism 8.0 Software.

Figure 6 A-B

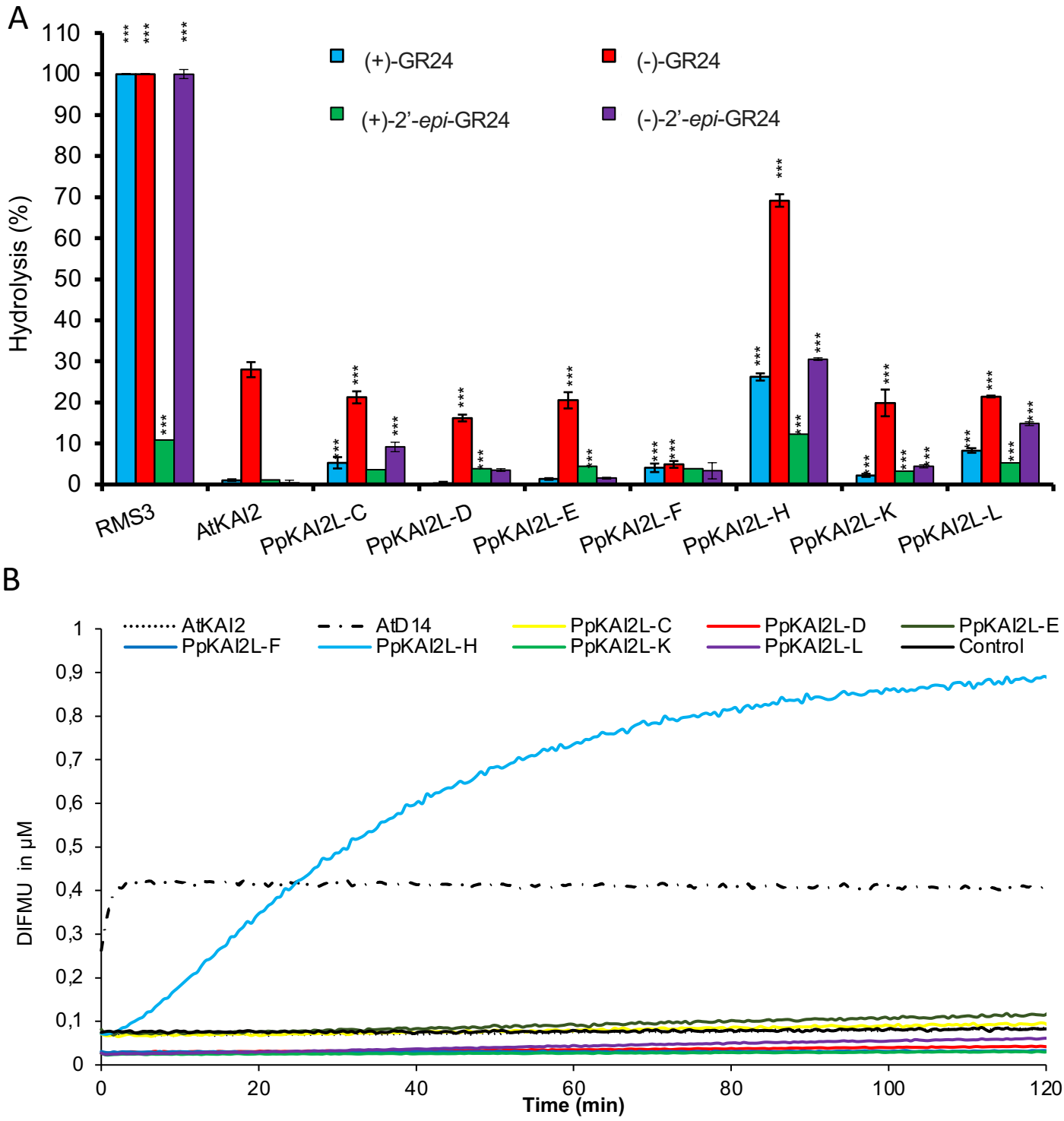
A
Hydrolysis (%)
(+)-GR24
(-)-GR24
(+)-2'-epi-GR24
(-)-2'-epi-GR24
RMS3
AtKAI2
PpKAI2L-C
PpKAI2L-D
PpKAI2L-E
PpKAI2L-F
PpKAI2L-H
PpKAI2L-K
PpKAI2L-L
B
AtKAI2
AtD14
PpKAI2L-C
PpKAI2L-D
PpKAI2L-E
PpKAI2L-F
PpKAI2L-H
PpKAI2L-K
PpKAI2L-L
Control
DIFMU in µM
Time (min)

Figure 6 C-F

C

aa position	28	126	136	155	159	195	220
PpKAI2L-A	F	Y	L	W	F	F	A
PpKAI2L-B	F	Y	F	W	F	F	A
PpKAI2L-C	F	Y	F	W	F	F	A
PpKAI2L-D	F	Y	F	W	F	F	A
PpKAI2L-E	F	Y	F	W	F	F	A
AtKAI2	F	Y	F	W	F	F	A
PpKAI2L-F	F	Y	F	W	F	F	A
PpKAI2L-K	F	Y	F	W	F	F	A
PpKAI2L-H	L	Y	F	W	F	F	A
PpKAI2L-I	F	Y	F	W	F	F	A
PpKAI2L-L	F	Y	F	W	F	F	A
PpKAI2L-J	F	Y	F	W	F	F	S
PpKAI2L-G	F	Y	F	W	F	F	S
PpKAI2L-M	F	Y	F	W	F	F	-
AtD14	F	F	F	W	F	F	S

D

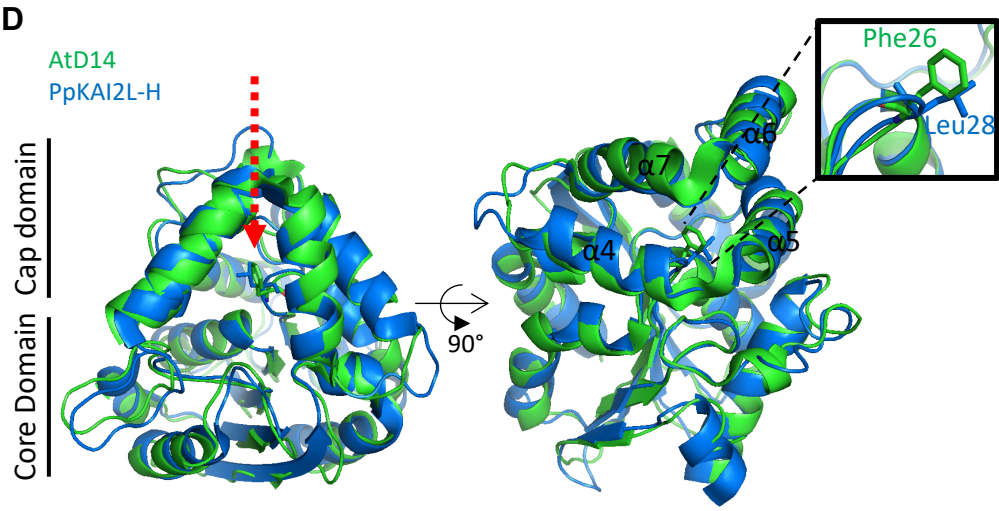

E

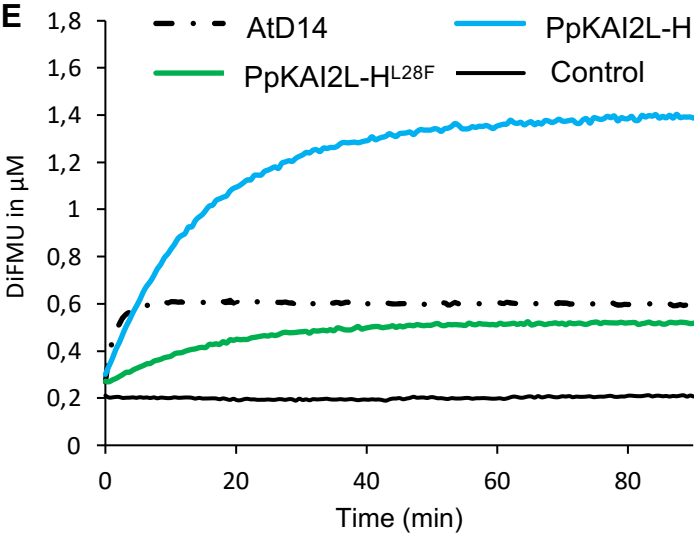

F

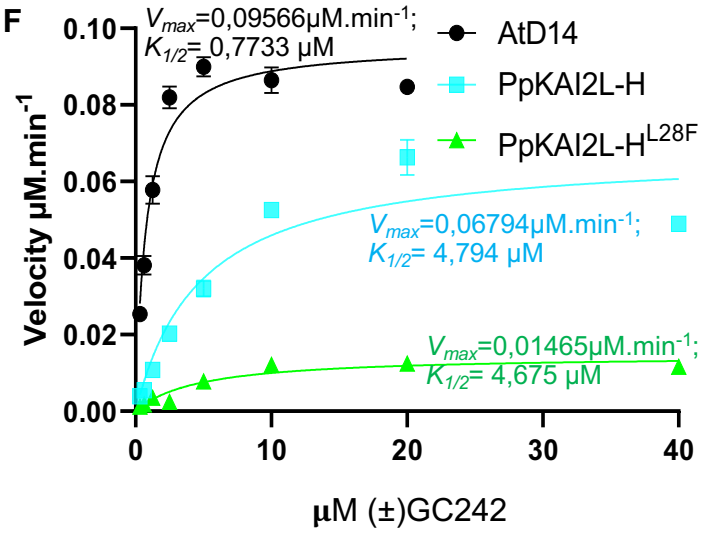

Figure 6: PpKAI2L enzymatic activities confirm stereoselectivity and reveal PpKAI2L-H special feature.

(A) PpKAI2L enzymatic activity towards GR24 isomers. (+)-GR24, (−)-GR24, (+)-2'-*epi*-GR24 and (−)-2'-*epi*-GR24 at 10 µM were incubated with 5 µM RMS3, AtKAI2 or the seven PpKAI2L proteins for 150 min at 25 °C. UPLC-UV (260 nm) analysis was used to detect the remaining amount of GR24 isomers. Columns represent the mean value of the hydrolysis rate calculated from the remaining GR24 isomers, quantified in comparison with (±)-1-indanol as internal standard. Error bars represent the SD of three replicates (means ± SD, n = 3). The asterisks indicate statistical significance from the AtKAI2 values, for each isomer, as ***$p \leq 0.001$; **$p \leq 0.01$ and n.s., $p > 0.05$, as measured by Dunnett nonparametric relative contrast effects test, with AtKAI2 considered as the control group, for each compound. **(B)** Enzyme kinetics for PpKAI2L, AtD14 and AtKAI2 incubated with (±)-GC242 (structure shown in Supplemental Figure 8A). Progress curves during probe hydrolysis, monitored (λ_{em} 460 nm) at 25 °C. Protein catalyzed hydrolysis with 330 nM of protein and 4 µM of probe**.** These traces represent one of the three replicates and the experiments were repeated two times. **(C)** Sequence alignment of active site amino acid residues in PpKAI2L proteins. Amino acids that differ from AtKAI2 are colored in red. A fully expanded alignment can be found in Supplemental Figure 2. **(D)** Superimposition of the AtD14 and PpKAI2L-H structure showing the position of the F^{28} and L^{28} residues. Zoom onto helices α4 and α5. **(E)** Enzyme kinetics for PpKAI2L-H, PpKAI2L-H^{L28F} and AtD14 incubated with (±)-GC242. Progress curves during probe hydrolysis, monitored (λ_{em} 460 nm) at 25 °C. Protein catalyzed hydrolysis with 330 nM of protein and 20 µM of probe**.** These traces represent one of the three replicates and the experiments were repeated two times. **(F)** Hyperbolic plot of pre-steady state kinetics reaction velocity with (±)-GC242. Initial velocity was determined with pro-fluorescent probe concentrations from 0.310 µM to 40 µM and protein at 400 nM. Error bars represent SE of the mean of three replicates and the experiments were repeated at least three times.

Figure 7

A

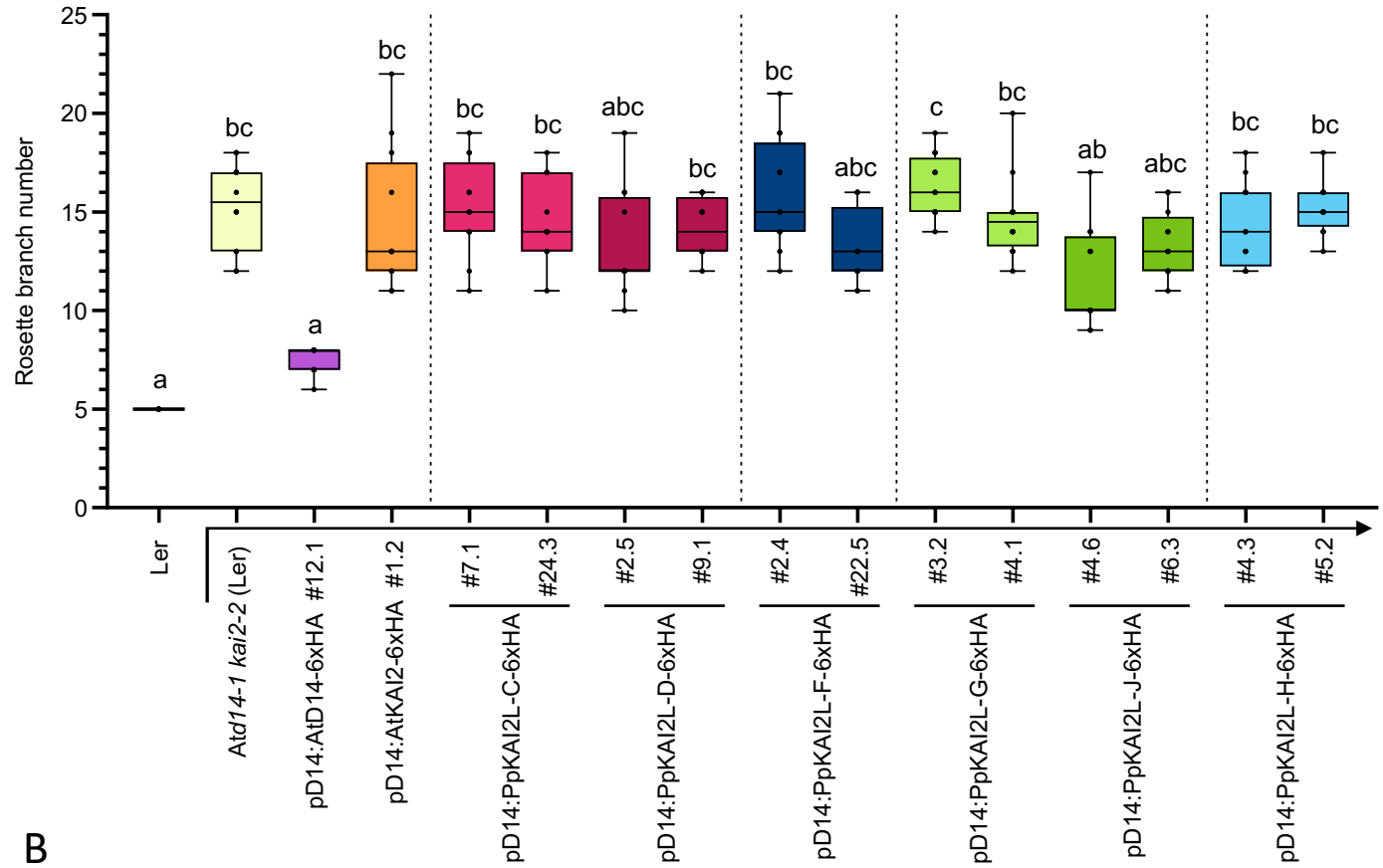
Rosette branch number
0
5
10
15
20
25
a
bc
a
bc
bc
bc
abc
bc
bc
abc
c
bc
ab
abc
bc
bc
Ler
Atd14-1 kai2-2 (Ler)
pD14:AtD14-6xHA #12.1
pD14:AtKAI2-6xHA #1.2
#7.1
#24.3
pD14:PpKAI2L-C-6xHA
#2.5
#9.1
pD14:PpKAI2L-D-6xHA
#2.4
#22.5
pD14:PpKAI2L-F-6xHA
#3.2
#4.1
pD14:PpKAI2L-G-6xHA
#4.6
#6.3
pD14:PpKAI2L-J-6xHA
#4.3
#5.2
pD14:PpKAI2L-H-6xHA

B

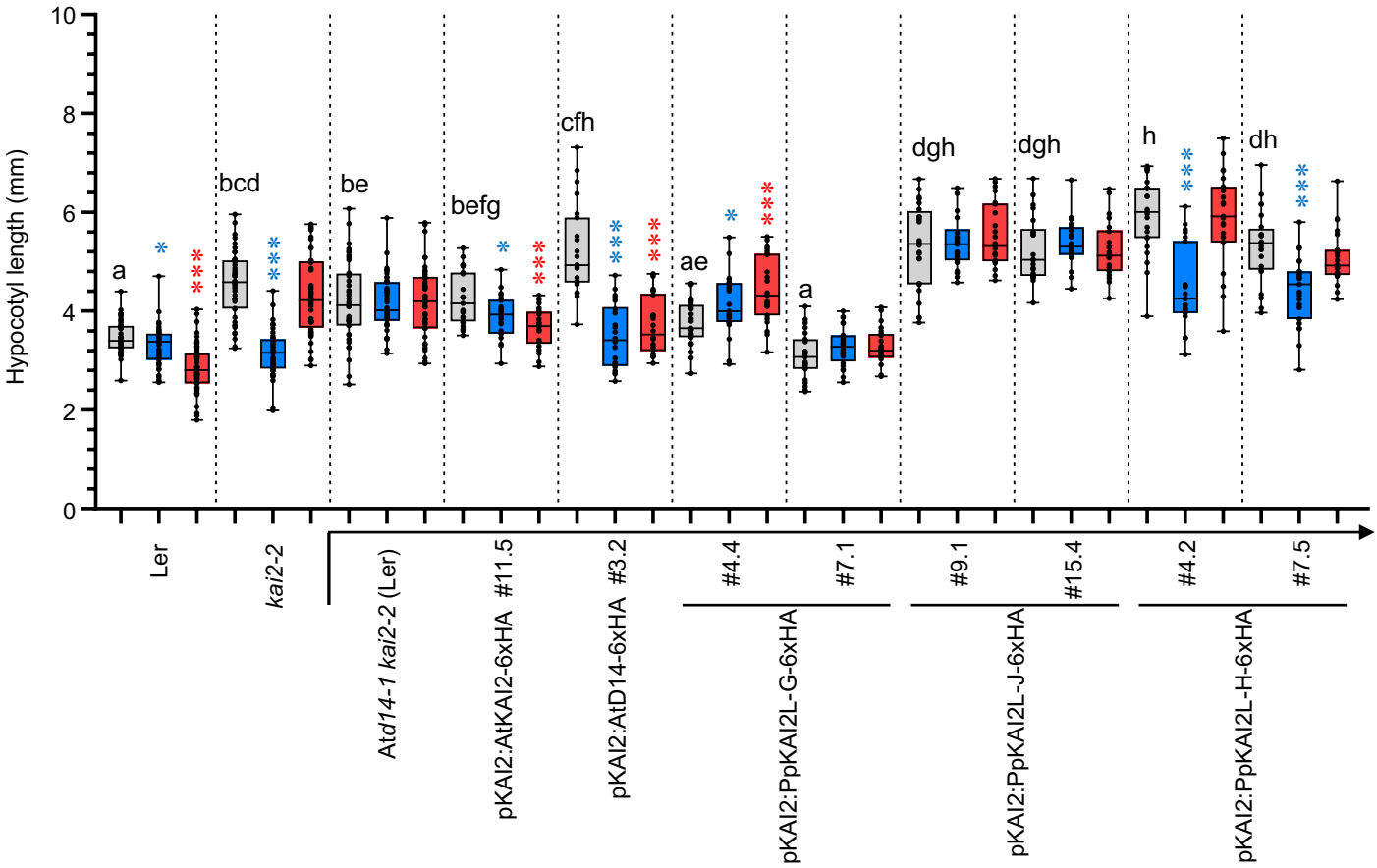
Hypocotyl length (mm)
0
2
4
6
8
10
a
bcd
be
befg
cfh
ae
a
dgh
dgh
h
dh
Ler
kai2-2
Atd14-1 kai2-2 (Ler)
pKAI2:AtKAI2-6xHA #11.5
pKAI2:AtD14-6xHA #3.2
#4.4
#7.1
pKAI2:PpKAI2L-G-6xHA
#9.1
#15.4
pKAI2:PpKAI2L-J-6xHA
#4.2
#7.5
pKAI2:PpKAI2L-H-6xHA

Figure 7: Complementation assays of the Arabidopsis At*d14-1 kai2-2 double* mutant with *PpKAI2L* genes.

Complementation assays of the At*d14-1 kai2-2* mutant (in Ler), transformed using the *AtD14* promoter **(A)** or *AtKAI2* promoter **(B)** to control At*D14*, *AtKAI2* (controls) or *PpKAI2L* gene expression as noted below the graph. Ler (WT), *kai2-2* and At*d14-1 kai2-2* mutants are shown as controls. **(A)** Number of rosette axillary branches per plant. Results are mean of n =12 plants per genotype, except for Ler and lines pD14:AtD14 #12.1 and pD14:PpKAI2L-C#24.3 (n = 11). Different letters indicate significantly different results between genotypes based on a Kruskal-Wallis test ($P < 0.05$, Dunn *post hoc* test with P values corrected following the Benjamini-Hochberg method). **(B)** Hypocotyl length under low light, on ½ MS medium with DMSO (control, grey bars) 1 mM (+)-GR24 (blue bars) or 1 mM (–)-GR24 (red bars). Different letters indicate significantly different results between genotypes in control conditions based on a Kruskal-Wallis test ($P < 0.05$, Dunn *post hoc* test with P values corrected following the Benjamini-Hochberg method). Symbols in blue and red give the statistical significance of response to (+)-GR24 and (–)-GR24 respectively (Mann-Whitney tests, * $0.01 \leq p < 0.05$, *** $p \leq 0.001$).

Figure 8

		Mutation type		Effect
PpKAI2L-A			21 β2 41	
WT	GAGATTGTTGTCCTCGGCCATG--GTTTTGGCACCGACCAGTCTGTGTGGA		EIVVLGHGFGTDQSVWKHVVP	
a1	GAGATTGTTGTCCTCGGCCATG--GT------ACCGACCAGTCTGTGTGGA	- 6bp	EIVVLGHG--TDQSVWKHVVP	- 2 AA
*a2**	GAGATTGTTGTCCTCGGCCATGACGTTTTGGCACCGACCAGTCTGTGTGGA	+ 2pb	EIVVLGHDVLAPTSL-/49/*	frame shift
*a3**	GAGATTGTTGTCCTCGGCCATG--G----------ACCAGTCTGTGTGGA	- 11bp	EIVVLGHGPVCVETCRTSPR*	frame shift
PpKAI2L-B			1 β1 19	
WT	ATGTGTCCGGGACCGACTC----------TGTTGGAGGCTCATAAT		MCPGPTLLEAHNVHVVGHG	
b1	ATGTGTCCGGGACCGAC----------TCATAAT	-12bp	MCPGPT----HNVHVVGHG	- 4
*b4**	ATGTGTCCGGGACCGAC----------ATGCTTCCATAC-TGTTGGAGGCTCA**TAA**T	-13bp;+12bp	MCPGPTCFHTVGGS*	frame shift
PpKAI2L-C			53 αB 72	
WT	GATAACATGGGAGCTGGCACCACCGACCCGGAGTATTTTAGCTTCTCGAGA		DNMGAGTTDPEYFSFSRYST	
c1	GATAAC----------CCGGAGTATTTTAGCTTCTCGAGA	-21bp	DN-------PEYFSFSRYST	- 7 AA
*c2**	GATAACATGGGAGCTGGCACCACC-----GGAGTATTT**TAG**CTTCTCGAGA	-5bp	DNMGAGTTGVF*	frame shift
*c3**	GATAACATGGGAGCTGGCACCACCGA-----AGTATTT**TAG**CTTCTCGAGA	-5bp	DNMGAGTTEVF*	frame shift
PpKAI2L-D			23 β2 42	
WT	GGTCATGGGTTCGGCACGGATCAATCTGTGTGGAAGCACGTCATTCCACAC		VVLGHGFGTDQSVWKHVIPH	
d1	GGTCATGGGTTCGGCACGGATCG---TGTGTGGAAGCACGTCATTCCACAC	-4bp;+1bp	VVLGHGFGTDR-VWKHVIPH	-1 AA & Q33R
*d3**	GGTCATGG----------AAGCACGTCATTCCACAC	-25bp	VVLGHGSTSFHTLSMSTV*	frame shift
*d4**	GGTCATGGGTTCGGCACGGATCAAT----------CCACAC	-20bp	VVLGHGFGTDQSTPCR*	frame shift
PpKAI2L-E			90 β4 αC 108	
WT	ATCTACGTTGGACATTCGGTGGCCG------GTATGGTTGGTTGTCTCGCATCGCT**TGA**		SCIYVGH**S**V-AGMVGCLASL	
e1	ATCTACGTTGGACATTCGGTGG---ACATTCGTATGGTTGGTTGTCTCGCATCGCT**TGA**	-3bp;+6bp	SCIYVGH**S**VDIRMVGCLASL	+1AA & AG99IR
*e2**	ATCTACGTTGGACATTC----------GTATGGTTGGTTGTCTCGCATCGCT**TGA**	-8bp	SCIYVGH**S**YGWLSRIA*	frame shift
PpKAI2L-F			17 β2 38	
WT	GGGTTTGGATCTGACCAGACGGTGTGGAAAT----------ACGTCTTGCCGTAT		VLSHGFGSDQTVWKYVLPYIMN	
*f1**	GGGTT----------TGGAAAT----------ACGTCTTGCCGTAT	-19pb	VLSHGFGNTSCRIS*	frame shift
*f2**	GGGT----------GTGGAAAT----------ACGTCTTGCCGTAT	-19pb	VLSHGCGNTSCRIS*	frame shift
PpKAI2L-K			225 αH β8 242	
WT	CCGCTCCAAGTGGCGAATTACATG-------GTACGGAACTTGGGAGGGTGGACGATGA		PLQVANYMVRNLGGWTMM	
*k1**	CCGCTCCAAGTGGCGAATTACATG**TAA**TTCCGTACGGAACTTGGGAGGGTGGACGA**TGA**	+7bp	PLQVANYM*	frame shift
*k2**	CCGCTCCAAGTGGCGAATTACATG-------TACGGAACTTGGGAGGGTGGACGA**TGA**	-1bp	PLQVANYMYGTWEGGR*	frame shif
PpKAI2L-H				
WT	CGCTTTTTCTTTCCAACTGCCTCGAAGAGATGCCGAGCCCGTTGC-//-ACTGCATCGACTCATGATCTATCCAAAACAGCCAT			CDS deletion
Δh	CGCTTTTTCTTTCCAACTGCCTCGAAGAGCTCGAGATAACTTC-/(LoxP)/-GAACTTATACTAGTCTATCCAAAACAGCCAT			
PpKAI2L-I			52 β3 69	
WT	CTGTTCGATATAATGGGAGCCGGCACTACGGACCCTGAGCACTTTAGCTCTAAGAGT		LFDIMGAGTTDPEHFSSK	
*i1**	CTGTTCGATATAATGGGAGCCG----------GCACTTTAGCTCTAAGAGT	-16bp	LFDIMGAGTLALR-/13/-RF*	frame shift
*i2**	CTGTTCGATATAATGGGAGCCGG----------AGCACTT**TAG**CTCTAAGAGT	-14bp	LFDIMGAGAL*	frame shift
*i3**	CTGTTCGATATAATGGGAGCCGGCAC-------CCTGAGCACTTTAGCTCTAAGAGT	-7bp	LFDIMGAGTLSTL-/16/-RF*	frame shift
PpKAI2L-L			54 β1 68	
WT	TTGTTAGCTGCCCACAATCTGAGTGTTCTGGGCAACGGCGACCAAGTT		LLAAHNLSVLGNGDQV	
*l1**	TTGTTA----------TCTGAGTGTTCTGGGCAACGGCGACCAAGTT	-11bp	LLSECSGQRRPSC/8/*	frame shift
l2	TTGTTAGCTGCCCA---TCTGAGTGTTCTGGGCAACGGCGACCAAGTT	-3bp	LLAAH-LSVLGNGDQV	-1AA
PpKAI2L-J			14 Not conserved 30	
WT	GACTTGTGCCACGAGAACCCTTAC-----CTGAAGGCTCACAACGTAAGTGTCTTC		DLCHENPYLKAHNVSVF	
*j1**	GACTTGTGCCACGAGAACCCTTACAACGT-TGAAGGCTCACAACGTAAGTGTCTTC	-6bp;+5bp	DLCHENPYNVEGSQ/20/*	frame shift
j3	GACTTGTGCC----------AC-----CTGAAGGCTCACAACGTAAGTGTCTTC	-12bp	DLCH----LKAHNVSVF	-4 AA
j4	GACTTGTGCCACGAGAACCCTTAC-----C----------ACGTAAGTGTCTTC	-12bp	DLCHENPY----NVSVF	-4 AA
j5	GACTTGTGCCACGAGAACCCTTAC----------TACGTAAGTGTCTTC	-13bp;+1bp	DLCHENPY----YVSVF	-4aa & N26Y
PpKAI2L-G			157 β6 αT1 175	
WT	CAGTAACGACGGAGATTACATCGGAGGGTTTGAGATGGAGGAGCTTCATGAGCTGTT		SNDGDYIGGFEMEELHELF	
g1	CAGTAACGA----------CGGAGGGTTTGAGATGGAGGAGCTTCATGAGCTGTT	-12bp	SND----GGFEMEELHELF	-4AA
*g2**	CAGTAACGACGGAGATTACAT----------GAGCTGTT	-28bp	**S**NDGDYMSCSPPCGQIS*	frame shift
*g3**	CAGTAACGACGGAGATTACATC----------	-64bp	SNDGDYI----------	-21AA
*g4**	CAGTAACGACGGAGAT-----GGAGGAGTT**TGA**GATGGAGGAGCTTCATGAGCTGTT	-11bp;+6bp	SNDGDGGV*	frame shift
PpKAI2L-M			157 β6 αT1 175	
WT	AGTAACGACGGAGATTACATCGGAGGGTTTGAGATGGAGGAGCTTCATGAGCTGTTC		SNDGDYIGGFEMEELHELF	
m1	AGTAACGA----------CGGAGGGTTTGAGATGGAGGAGCTTCATGAGCTGTTC	-12b	SND----GGFEMEELHELF	-4AA
*m2**	AGTAACGACGGAGATTACAT-GGAGGGTTTGAGATGGAGGAGCTTCATGAGCTGTTC	-1bp	SNDGDYMEGLRW/12/IS*	frame shift
*m6**	AGTAACGACGGAGATTACATCGG----TTTGAGATGGAGGAGCTTCATGAGCTGTTC	-4bp	SNDGDYIGLRW/12/IS*	frame shift

Figure 8: Mutations obtained in all 13 *PpKAI2L* genes.
For all 13 *PpKAI2L* genes, the WT nucleotide and protein sequences are shown above the altered sequences found in the generated CRISPR-Cas9 lines (in italics, numbered). The number of the first shown amino acid (aa) and the predicted secondary structure are indicated above the WT protein sequence. The sgRNA sequence is shown in blue, with the PAM site underlined. Deletions are shown as dashes, insertions are noted with orange letters. The mutation type is shown on the right. Premature STOP codons are noted in bold, and with a red star on the aa sequence. On protein sequences, the number of not shown aa is noted between slashes. For *PpKAI2L-E*, the serine (S) of the catalytic triad is noted in bold blue. For *PpKAI2L-H*, a deletion of the full coding sequence between the ATG and STOP was obtained through homologous recombination; the use of CRE recombination led to 46 residual nucleotides, (not shown) corresponding to the LoxP site (see Materials and Methods). See Supplemental Table 2 for the list of mutants carrying one or several of the shown mutations.

Figure 9

A

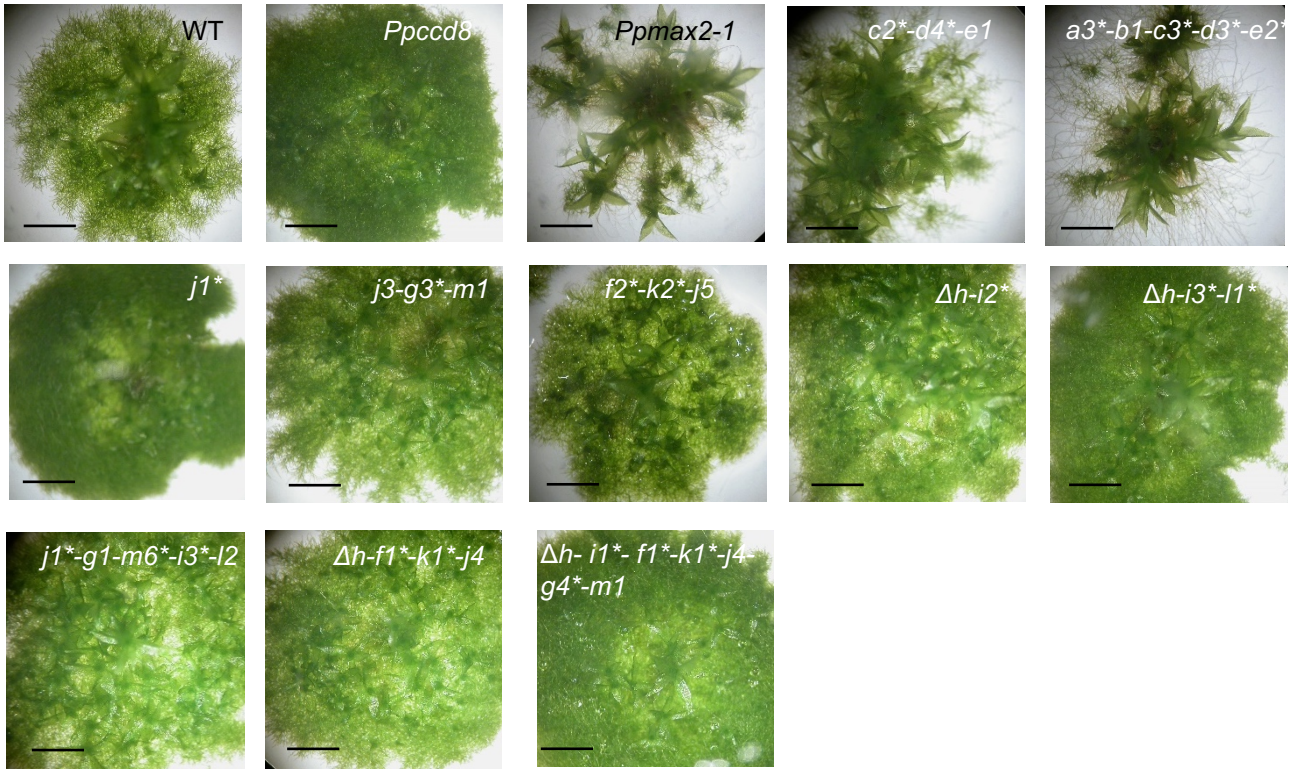
WT
Ppccd8
Ppmax2-1
c2*-d4*-e1
a3*-b1-c3*-d3*-e2*
j1*
j3-g3*-m1
f2*-k2*-j5
Δh-i2*
Δh-i3*-l1*
j1*-g1-m6*-i3*-l2
Δh-f1*-k1*-j4
Δh- i1*- f1*-k1*-j4-g4*-m1

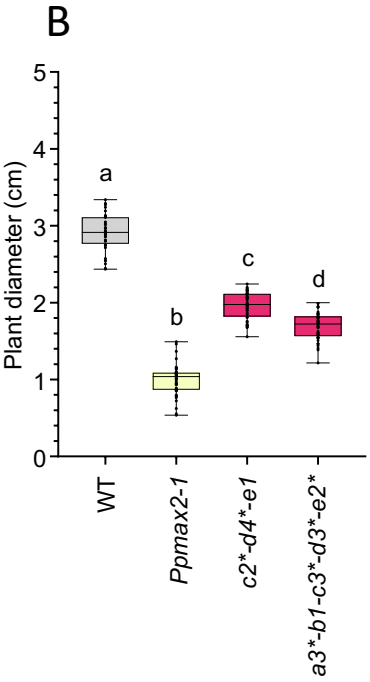
B
Plant diameter (cm)
0
1
2
3
4
5
a
b
c
d
WT
Ppmax2-1
c2*-d4*-e1
a3*-b1-c3*-d3*-e2*

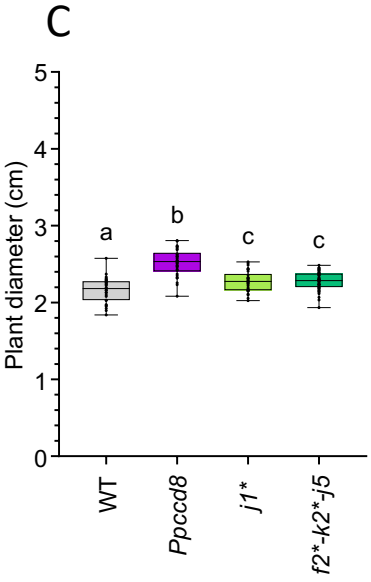
C
Plant diameter (cm)
0
1
2
3
4
5
a
b
c
c
WT
Ppccd8
j1*
f2*-k2*-j5

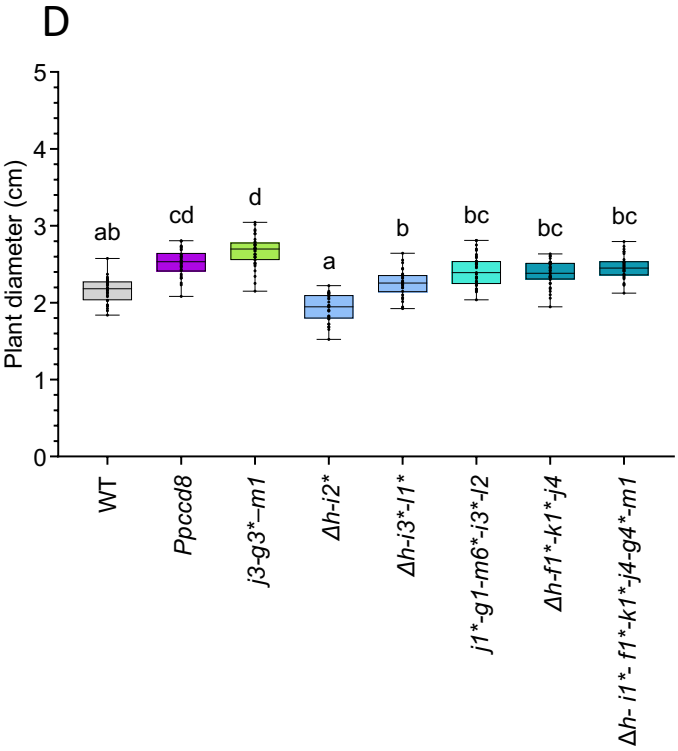
D
Plant diameter (cm)
0
1
2
3
4
5
ab
cd
d
a
b
bc
bc
bc
WT
Ppccd8
j3-g3*–m1
Δh-i2*
Δh-i3*-l1*
j1*-g1-m6*-i3*-l2
Δh-f1*-k1*-j4
Δh- i1*- f1*-k1*-j4-g4*-m1

Figure 9: Phenotype of the *Ppkai2L* mutants in light.
Plant diameters were measured after four weeks growth in the light. **(A)** 3-week-old plants. Scale bar = 2 mm **(B)** and **(C)**: 30-day-old plants, n > 40; (D): 28-day-old plants, n = 30. **(B)**, **(C)** and **(D):** All plants were grown on cellophane disks. Letters indicate statistical significance of comparisons between all genotypes (Kruskal-Wallis test followed by a Dunn *post hoc* test ($p < 0.05$)).

Figure 10

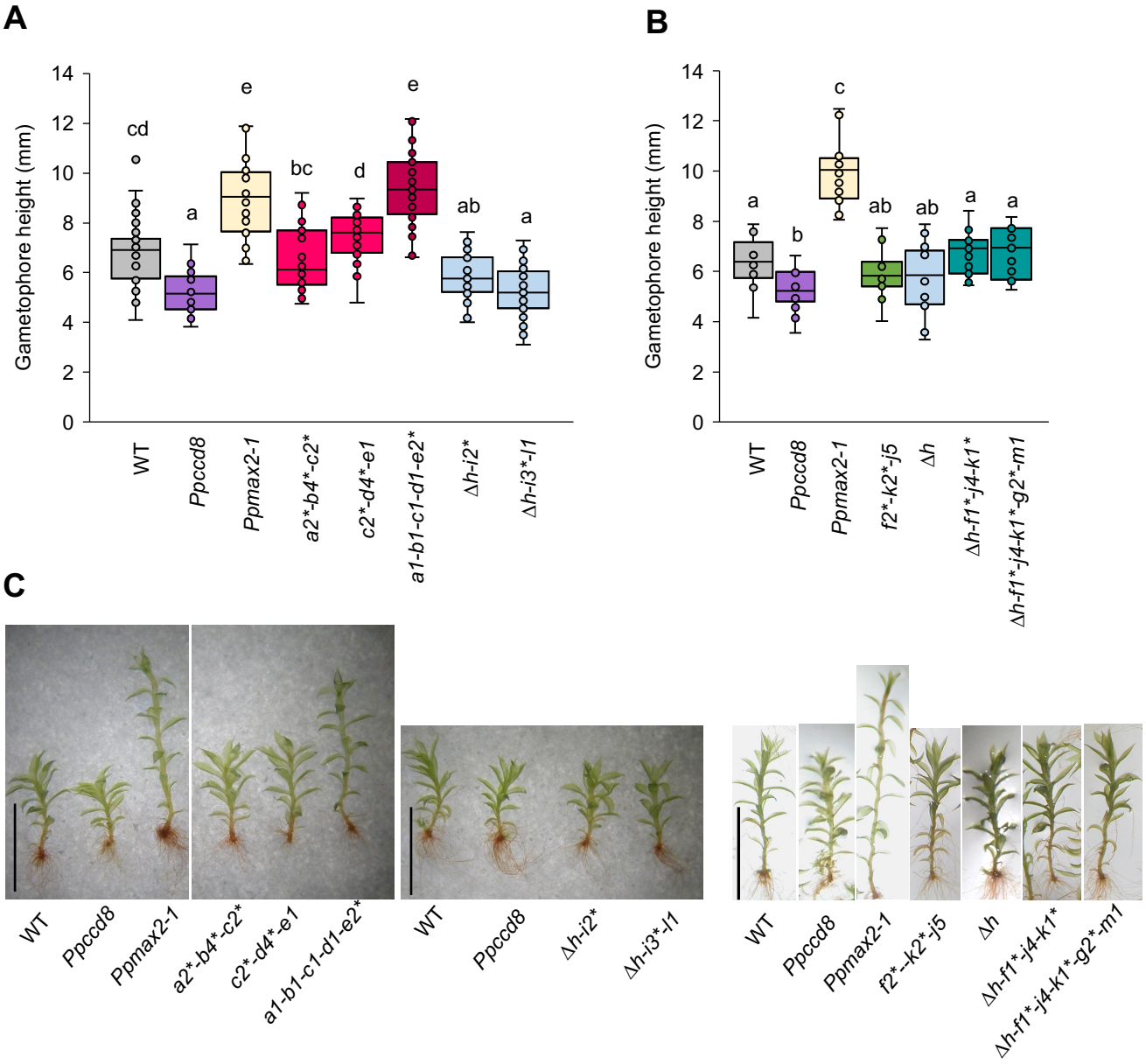
A
Gametophore height (mm)
0
2
4
6
8
10
12
14
cd
a
e
bc
d
e
ab
a
WT
Ppccd8
Ppmax2-1
a2*-b4*-c2*
c2*-d4*-e1
a1-b1-c1-d1-e2*
Δh-i2*
Δh-i3*-l1
B
Gametophore height (mm)
a
b
c
ab
ab
a
a
WT
Ppccd8
Ppmax2-1
f2*-k2*-j5
Δh
Δh-f1*-j4-k1*
Δh-f1*-j4-k1*-g2*-m1
C
WT
Ppccd8
Ppmax2-1
a2*-b4*-c2*
c2*-d4*-e1
a1-b1-c1-d1-e2*
WT
Ppccd8
Δh-i2*
Δh-i3*-l1
WT
Ppccd8
Ppmax2-1
f2*--k2*-j5
Δh
Δh-f1*-j4-k1*
Δh-f1*-j4-k1*-g2*-m1

Figure 10: *Ppkai2L* mutant gametophores in red light.
(A) Gametophore height of *Ppkai2L* mutants affecting clade (A-E) genes (*a2*-b4*-c2*; c2*-d4*-e1; a1-b1-c1-d1-e2**) and clade (HIL) genes (Δ*h-i2** and Δ*h-i3*-l1*), compared to that of WT, *Ppccd8* and *Ppmax2-1* mutants, following two months growth under red light. Mutant genotypes carry mutations as indicated in Figure 8 and Supplemental Table 2, with asterisks for null mutations. Box plots of n = 32-36 gametophores, grown in three Magenta pots, harboring between 15 and 25 leaves. Statistical groups (all genotypes comparison) are indicated by letters and were determined with a Kruskal-Wallis test followed by a Dunn *post hoc* test ($p<0.05$). **(B)** Gametophore height of *Ppkai2L* mutants affecting clade (HIL) gene (Δ*h*), both clades (FK) and (JGM) (*f2*-j5*-k2**) and all three clades (HIL) (FK) and (JGM) (Δ*h-f1*-j4-k1** and Δ*h-f1*-j4-k1*-g2*-m1)*. Mutant genotypes carry mutations as indicated in Figure 8 and Supplemental Table 2, with asterisks for null mutations. Box plots of n = 11-15 gametophores, grown in three Magenta pots, harboring between 15 and 25 leaves. Statistical groups (all genotypes comparison) are indicated by letters and were determined with a Kruskal-Wallis test followed by a Dunn *post hoc* test ($p < 0.05$). **(C)** Examples of gametophores following two months growth under red light, from WT, *Ppccd8*, *Ppmax2-1*, and *Ppkai2L* mutants as shown in (A) and (B). Scale bar = 5 mm.

Figure 11

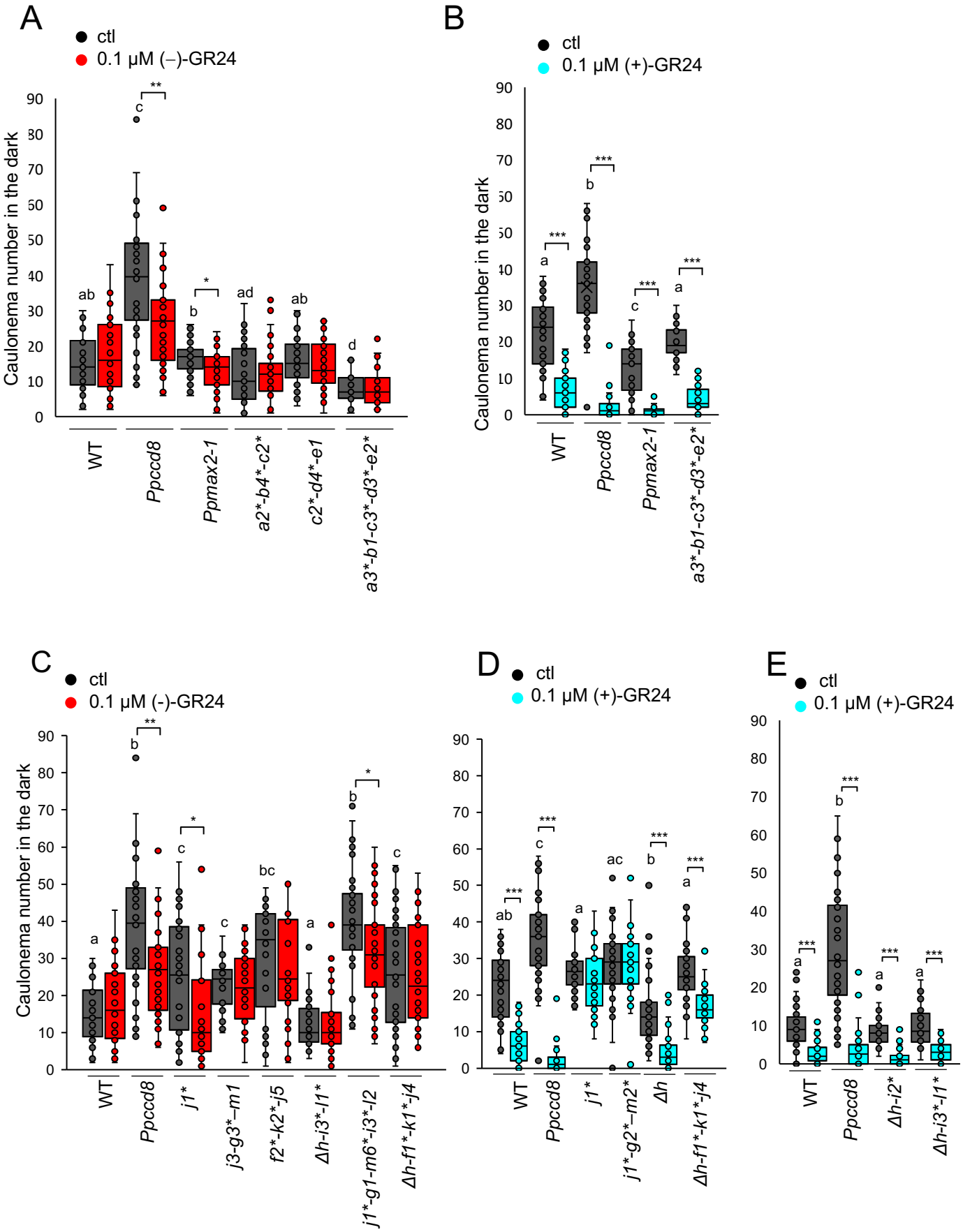
A
ctl
0.1 μM (−)-GR24
Caulonema number in the dark
WT
Ppccd8
Ppmax2-1
a2*-b4*-c2*
c2*-d4*-e1
a3*-b1-c3*-d3*-e2*
B
ctl
0.1 μM (+)-GR24
Caulonema number in the dark
WT
Ppccd8
Ppmax2-1
a3*-b1-c3*-d3*-e2*
C
ctl
0.1 μM (-)-GR24
Caulonema number in the dark
WT
Ppccd8
j1*
j3-g3*–m1
f2*-k2*-j5
Δh-i3*-l1*
j1*-g1-m6*-i3*-l2
Δh-f1*-k1*-j4
D
ctl
0.1 μM (+)-GR24
WT
Ppccd8
j1*
j1*-g2*–m2*
Δh
Δh-f1*-k1*-j4
E
ctl
0.1 μM (+)-GR24
WT
Ppccd8
Δh-i2*
Δh-i3*-l1*

Figure 11: Phenotypic response of *Ppkai2L* mutants to (-)-GR24 and (+)-GR24 application: *caulonema* number in the dark.

(**A-B**) *Caulonema* numbers from mutants affecting clade (A-E) genes following application of 0.1 µM (–)-GR24 (in red, **A**) or 0.1µM (+)-GR24 (in turquoise, **B).** DMSO was applied as a control treatment (ctl, dark grey). WT and both the *Ppccd8* and *Ppmax2-1* mutants were used as control genotypes. (**C-E**) *Caulonema* numbers from mutants affecting clade (JGM) genes: *j1*; j3-g3*-m1; j1*-g2*-m2*;* clade (FK) and (JGM) genes: *f2*-k2*-j5, clade* (HIL) genes: *Δh, Δh-i2*, Δh-i3*-l1*,* clade (HIL) and (JGM) genes: *j1*-g1-i3*-l2,* or all 3 clades genes: *Δh-f1*-j4-k1**, following application of 0.1µM (–)-GR24 (in red, **C**) or 0.1µM (+)-GR24 (in turquoise, **D, E**). 0.01% DMSO was applied as a control treatment (ctl, dark grey). WT and the *Ppccd8* mutant were used as control genotypes. Mutant genotypes carry mutations as indicated in Figure 8 and Supplemental Table 2, with asterisks for null mutations. For each genotype, *caulonema* were counted after two weeks in the dark, from 24 individuals, grown in three different 24-well plates. Statistical groups (comparing genotypes in control conditions) are indicated by letters and were determined by a one-way ANOVA with Welch test (95% Cl). Significant differences between control and treated plants within a genotype based on one-way ANOVA with Welch test: ***, $p < 0.001$; **, $p < 0.01$; *, $p < 0.5$; $p < 0.1$.

Figure 12

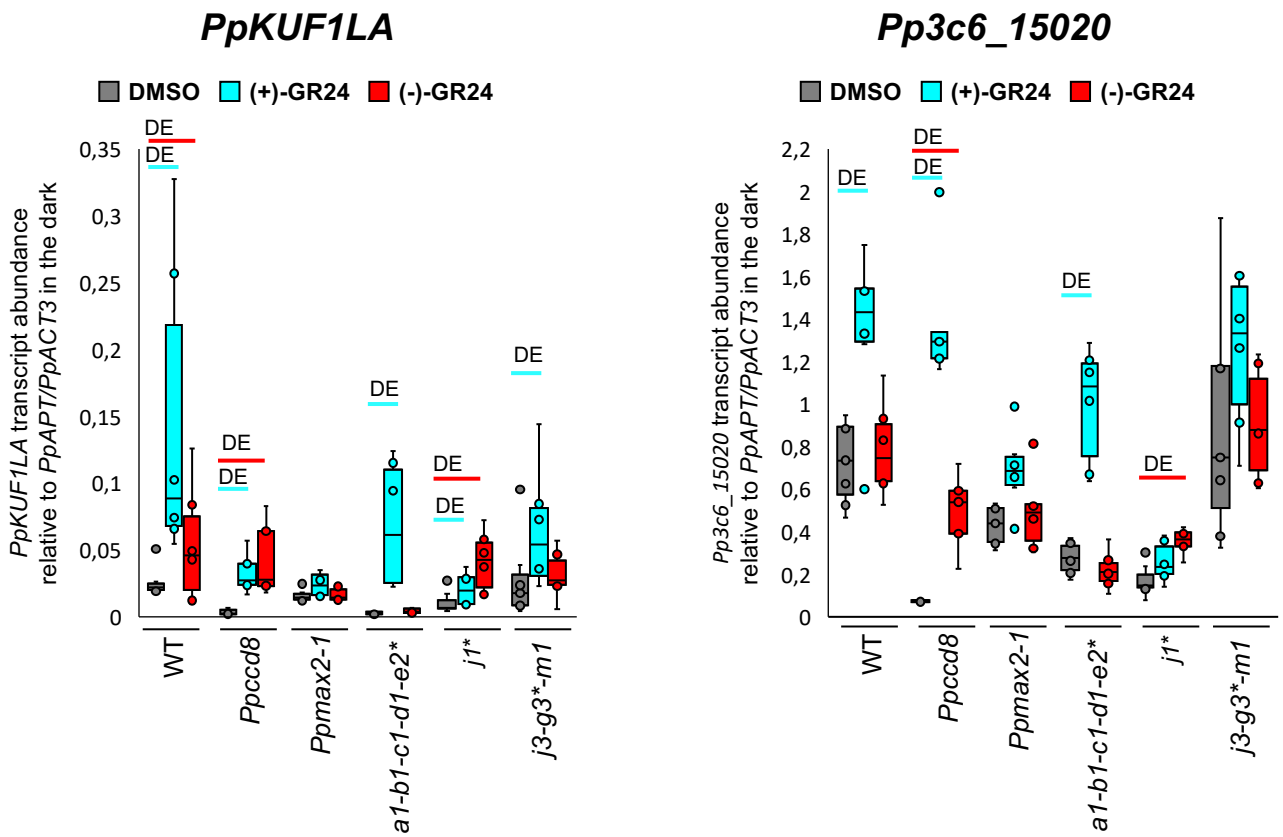

Figure 12: *Ppkai2l* mutant transcriptional response to (+)-and (−)-GR24.
Transcript abundance analysis of the SL-responsive genes *PpKUF1LA* and *Pp3c6_15020,* in WT*, Ppccd8, Ppmax2-1* and *Ppkai2L* mutants *a1-b1-c1-d1-e2** (clade (A-E)), j1* and j3-g3*-m1 (clade (JGM)), grown for two weeks in light, then transferred for one week in the dark*,* six hours after treatment with DMSO (control, grey plots), 1 µM (+)-GR24 (turquoise plots) or 1 µM (−)-GR24 (red plots). Box plots of at least four biological repeats are shown, relative to mean (*PpAPT-PpACT3*) transcript abundance. Two-fold differences in median values of transcript levels between control and treated plants are estimated as significant (DE) and noted in corresponding colors (turquoise for (+)-GR24 and red for (−)-GR24).

Figure 13

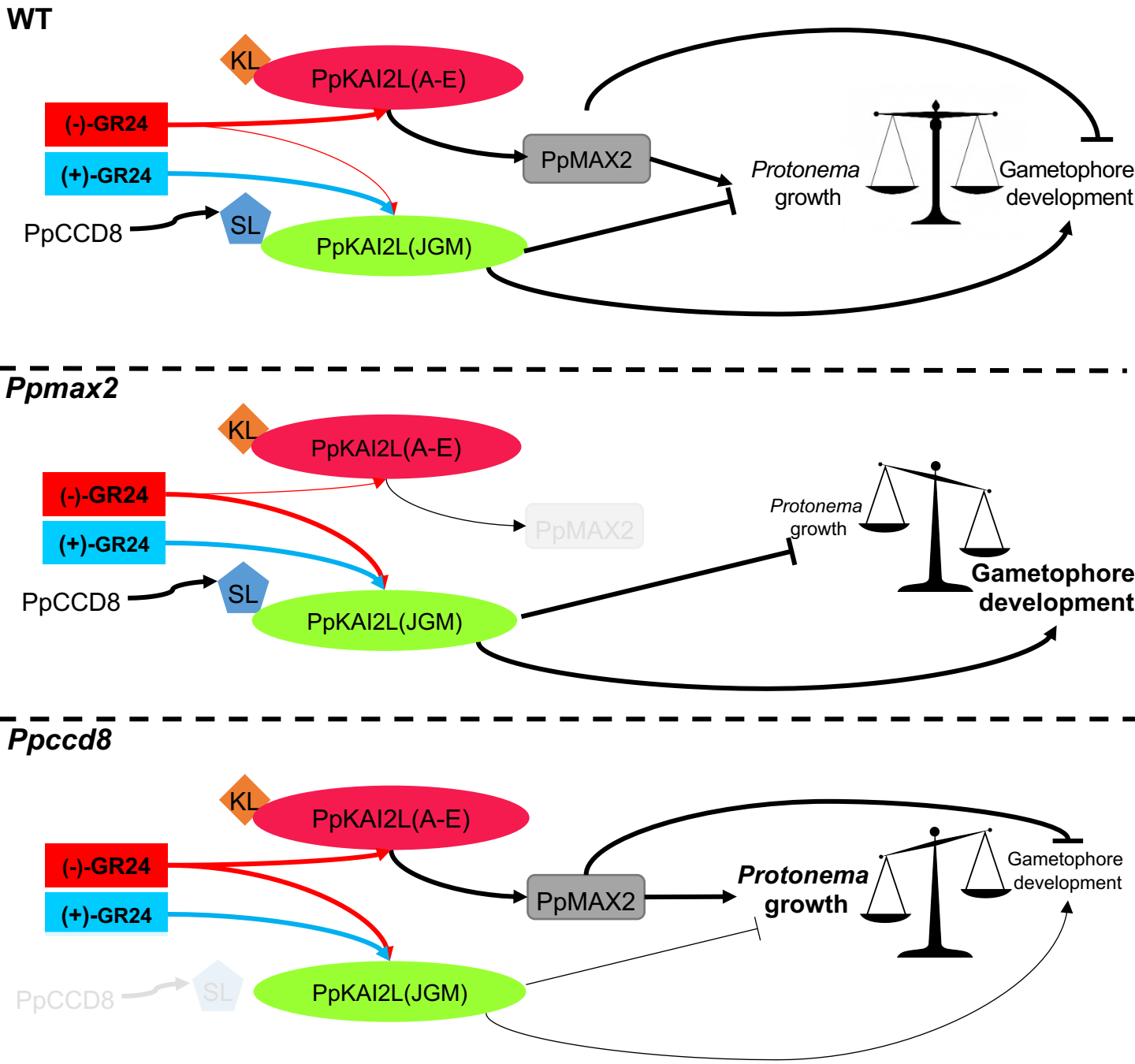

Figure 13: Current model for SL (PpMAX2-independent) and KL (PpMAX2-dependent) perception in *P. patens*.

The WT moss phenotype is the outcome of a balance between protonema growth and gametophore development. Clade (A-E) PpKAI2L proteins perceive KL compounds which promotes protonema growth and inhibits gametophore development through a PpMAX2-dependent pathway. Clade (JGM) PpKAI2L proteins perceive PpCCD8-derived compounds (noted SL) which inhibits protonema growth while promoting gametophore development, in a PpMAX2-independent manner. The phenotypes of *Ppmax2* (early gametophores) and *Ppccd8* (extended protonema) mutants are the result of an upset in this balance between protonema growth and gametophore development. (+)-GR24 mimics PpCCD8-derived compound effects. (–)-GR24 is perceived by both clade (A-E) and clade (JGM) PpKAI2L proteins and is a poor mimic of moss KL.